Available online at www.sciencedirect.com
SCIENCE DIRECT®
Journal of Computational Physics 190 (2003) 651–681
JOURNAL OF COMPUTATIONAL PHYSICS
www.elsevier.com/locate/jcp

# Ghost fluid method for strong shock impacting on material interface

T.G. Liu [a], B.C. Khoo [b,c,*], K.S. Yeo [b]

[a] Institute of High Performance Computing #01-01 The Capricorn, Singapore Science Park II, Singapore 117528, Singapore
[b] Department of Mechanical Engineering, National University of Singapore, Singapore 119260, Singapore
[c] Singapore-MIT Alliance, 4 Engineering Drive 3, National University of Singapore, Singapore 117576, Singapore

Received 29 April 2002; received in revised form 9 April 2003; accepted 26 May 2003

**Abstract**

It is found that the original ghost fluid method (GFM) as put forth by Fedkiw et al. [J. Comp. Phys. 152 (1999) 457] does not work consistently and efficiently using isentropic fix when applied to a strong shock impacting on a material interface. In this work, the causes for such inapplicability of the original GFM are analysed and a modified GFM is proposed and developed for greater robustness and consistency. Numerical tests also show that the modified GFM has the property of reduced conservation error and is less problem-related.


## 1. Introduction

A relatively dominant difficulty for simulating compressible multi-medium flow is the treatment of moving material interfaces and their vicinity. In general, there are two basic approaches to treat such contact discontinuities. The first, front capturing, represents contact discontinuities as steep gradients to be resolved over a few grid cells. The other approach is front tracking in which contact discontinuities are treated as internal moving boundaries.

A main advantage for employing front capturing is its relative simplicity and ease of extension to multi-dimensions. Solvers used to obtain the flow field are normally high-resolution schemes like TVD, ENO and WENO in order to handle possible shock waves. When such a scheme is employed to solve multi-material flow, however, numerical inaccuracies and oscillations can occur at the material interfaces. Various techniques have been developed to overcome these difficulties like Larrouturou [20], Karni [18], Abgrall [3], Jenny at el. [17], Cocchi and Saurel [6] and others. A good summary may be found in [4]. Due to numerical smearing at the material interface, inaccurate boundary conditions are actually enforced at the moving

* Corresponding author. Tel.: +65-874-2889; fax: +65-779-1459.
*E-mail addresses:* liutg@ihpc.a-star.edu.sg (T.G. Liu), mpekbc@nus.edu.sg (B.C. Khoo).

0021-9991/$ - see front matter © 2003 Elsevier B.V. All rights reserved.
doi:10.1016/S0021-9991(03)00301-2

interface; a jump value such as density, viscosity and tangential velocity is therefore non-physically enforced to be continuous across the said smeared interface [26,27]. Such an implementation can cause non-physical compression in the interface region during the simulation of incompressible flow. Another disadvantage of front capturing is the possible inaccuracy of wave interaction occurring at the interface, which is again due to numerical smearing. For instance, a shock-induced cavitation region may not be faithfully captured in the simulation of an underwater shock interacting with a free surface. The appearance of cavitation could affect the pressure loading on a nearby underwater structure [23].

The algorithm developed by Glimm et al. [8] is a good representative of front tracking. In front tracking, accurate boundary conditions can be imposed at the moving interfaces. Moreover, the non-physical compression can be relatively easy to avoid in the simulation of incompressible flow. On the other hand, a front tracking approach is usually quite complex in order to be able to treat large interfacial deformation. At times reconstruction of the tracked interface is required [19,28]. Another disadvantage arising from the use of front tracking is the possible numerical instability caused by the presence of extremely small grid sizes/volumes. To remove such instability, solution redistribution [16,21] or cell merging/splitting [11] has to be employed. Such additions can further contribute to an already quite complicated extension to multi-dimensions. Furthermore, a front tracking approach may be non-conservative although maintenance of conservation is not necessarily important for front tracking once accurate boundary conditions are imposed at the interface. Recently, efforts have been made on this topic [9]; however, much work has yet to be carried out for a fully conservative front tracking approach in multi-dimensions.

Recently, efforts also have been made to combine advantages of both front tracking and front capturing to resolve wave interaction at the gas–water interface [21]. Specifically, detailed treatment of interface evolution was avoided by employing the level set technique with the proviso that smearing at the interface was not allowed to ensure accurate shock wave–interface interaction. To treat the wave interaction at the interface, an implicit characteristic method based on ARPS (approximate Riemann problem solver) was developed. The extension of this method to multi-dimensions can be achieved via integral conservation laws or dimension splitting technique. If the dimension splitting method is employed, fairly complex treatment is required for the situation of interface moving away from a grid line in the direction of sweep [22].

The ghost fluid method (GFM) [13] presented a fairly simple way for the extension to multi-dimensions. In the GFM, the level set technique is employed to capture the moving interface. A band of 3–5 grid points as ghost cells is defined in the vicinity of the interface. At the ghost cells, ghost fluid and real fluid co-exist; the ghost fluid is defined with the pressure and (normal) velocity as for the real fluid and the density is obtained from isobaric (usually isentropic) fixing technique [12]. The GFM allows calculation in the interface region as if in a single medium domain. Thus, numerical oscillations, which usually occur in a Eulerian method as applied to multi-medium flow, are generally eliminated. By discarding one side of the computation at the ghost points with respect to the new interface position obtained via the level set technique, a sharp contact discontinuity is then maintained. The GFM makes the interface "invisible" during the computation of flow field such that its extension to multi-dimensions becomes fairly simple. Henceforth, we call the GFM as enunciated in [13] the original GFM, where the (normal) velocity and pressure of ghost fluid status are taken from the real fluid.

To apply the GFM to a general discontinuity moving at a speed in the normal direction such as for a detonation discontinuity [14] or a flame front [24], appropriate Riemann problems in a node by node fashion have been constructed and solved by implicitly imposing the Rankine–Hugoniot jump conditions. If the ghost fluid status is defined as for the original GFM, it was found to be less efficient and harbour some inaccuracies when applied to the gas–water flow [15]. Fedkiw [15], therefore, proposed a new version of GFM, which may overcome the difficulty encountered by the original GFM used for the gas–water flow and also those problems associated with the shock impact on the gas–water interface like Cases 3 and 4 to be presented in Section 4.3. However, a complete analysis for the new version of GFM is not the intent of the present study and is left to the future work. In this work, our focus is on analysing the behaviour of the

original GFM used in the treatment of possible pressure and (normal) velocity discontinuities due to shock impacting on an interface. Physically, the interface recovers to its normal motion instantly after a shock impacting. However, it takes a few or many computational steps as necessary to reach this state numerically. (Here, normal motion means that the pressure and normal velocity are continuous across the interface.) It is usually within these critical steps that numerical errors may accumulate to a degree that even causes breakdown of computation if no special effort is made. The original GFM has been shown to work well for shock tube problems and even a not-very-strong shock impacting on an interface. Such a GFM, however, does not work very efficiently in the application to a strong shock wave impacting on an interface (see Section 2.1). In such a situation, the pressure, velocity and entropy at the interface may experience a sudden jump; the sudden jump of pressure, velocity and entropy across the interface implies that the real fluid pressure and velocity may not readily be taken as "reasonably acceptable" ghost fluid pressure and velocity and thus these have to be predicted separately and correctly before the GFM is applied. Furthermore, the employment of Rankine–Hugoniot conditions only ensures the flow dynamic behaviour at the interface (contact discontinuity) (i.e., the continuity of pressure and normal velocity). At the moment of a shock impacting on the interface, a singularity is created at the interface, where the velocity and pressure are discontinuous. This singularity has to be correctly decomposed simultaneously, while the single utilisation of the Rankine–Hugoniot conditions is insufficient to fully determine the final interfacial status. In the singularity decomposition, the material properties play a very important role to determine the final interfacial dynamic parameters and entropy. Thus, the influence of material properties and wave interaction has to be taken into account in the construction of the ghost fluid status in such a situation. The motivation of the present work is to analyse fully the plausible causes for the inapplicability of the original GFM in such situations, and thereafter to propose a modified GFM to overcome the difficulties described above and yet lead to reasonably valid results. It was discussed in [13] that the isentropic fix, which is physically more natural, is not favourable for the water medium; the internal energy fix was suggested and used for water. It is the intent of this work to seek improvement to the GFM to work consistently for a given condition of isentropic fix, irrespective of the medium like gas or water and hence become less problem-related.

The text is arranged as follows. In Section 2, we will first provide some examples, where the original GFM gives rise to inaccurate results in the employment of isentropic fixing. Next, an analysis of the inability of the original GFM to provide accurate results for a strong shock impacting on an interface is given. In Section 3, a proposed modification to the original GFM is developed to overcome these difficulties. The conservation error is also discussed for both the original and modified GFMs. In Section 4, various challenging tests are carried out employing the original and modified GFMs for comparisons and further discussions. The problems relating to shock refraction as studied in this section are fairly non-trivial and may also be used to evaluate the robustness of other numerical methods for compressible multi-medium flow. Finally, a brief summary is given in Section 5.

## 2. The original GFM on shock refraction

A 1D analysis is given to provide some insight as to why the original GFM does not work efficiently using isentropic fix in certain situations. The 1D Euler equation can be written as

$$\frac{\partial U}{\partial t}+\frac{\partial F(U)}{\partial x}=0, \tag{2.1}$$

where $U=[\rho,\rho u,E]^{\mathrm{T}}$, $F(U)=[\rho u,\rho u^2+p,(E+p)u]^{\mathrm{T}}$, $\rho$ is the density, $u$ is the velocity, $p$ is the pressure and $E$ is the total energy. The total energy is given as

$$E=\rho e+\rho u^2/2, \tag{2.2}$$

where $e$ is the specific internal energy. For closure of system, the equation of state (EOS) is required. We assume that the EOS used in this work has the form, which is equivalent to the Mie–Gruneison family of equations of state

$$\rho e = f(\rho)p + g(\rho). \tag{2.3}$$

Here, $f$ and $g$ are functions of density and some constants associated with heat conductivity. In this work, we shall focus on three types of EOS. The first one is the $\gamma$-law for perfect gases, where $f = 1/(\gamma - 1)$ and $g = 0.0$. The second one is the Tait's EOS for water, which has the form of $p = B[\rho/\rho_0]^N - B + A$, where $N = 7.15$, $A = 1.0 \times 10^5$ Pa, $B = 3.31 \times 10^8$ Pa and $\rho_0 = 1000.0$ kg/m$^3$. The Tait's EOS can also be written in the form of (2.3) with $f = 1/(N-1)$ and $g = N(B-A)/(N-1)$. The third one is the JWL EOS for explosives. Details of these three types of EOS can be found in [13].

Next, we shall provide some 1D examples, where the original GFM does not work too well. Let us consider a shock wave impacting on an interface from medium 2 (see Fig. 1). We assume that the pressure and velocity of both media to be constant and equal initially, and denoted by $p_1$ and $u_1$ respectively. The governing equation is Eq. (2.1) with the initial conditions given as

$$U|_{t=0} = \begin{cases} U_4, & x < x_{0s}, \\ U_{02}, & x_{0s} < x < x_0, \\ U_{01}, & x > x_0, \end{cases} \tag{2.4}$$

where $U_4$ is the status behind the incident shock and satisfies the Rankine–Hugoniot conditions of $F(U_4) - F(U_{02}) = s_4(U_4 - U_{02})$. Here, $s_4$ is the speed of the incident shock. $x_0$ and $x_{0s}$ are the initial locations of the interface and incident shock, respectively. $U_{02}$ is the flow status ahead of the incident shock and $U_{01}$ is the initial status of medium 1. All parameters appeared are assumed to be non-dimensional unless otherwise stated. The basic scheme used is MUSCL. Isentropic fixing is employed. The computational domain is $[0.0, 1.0]$ with 201 uniform mesh and CFL is set to be 0.90. It should be mentioned that, in [13], an ENO solver was utilised which is different from the present MUSCL. As such, there can arise different numerical accuracy and errors involved. On the other hand, one will note that the analysis and discussion made in Section 2.3 are independent of the numerical scheme used. It is worth noting that in [13], internal energy fixing was specifically employed for the water medium instead of isentropic fixing. As it is the intent of the present work to have a singular condition irrespective of the medium involved, the isentropic fix is also applied for water medium in the original GFM calculation for comparison to the proposed modified GFM (Section 3) where isentropic fix is used throughout.

### 2.1. Some examples on application of the original GFM

*Case 1 – strong shock impacting on a gas–gas interface:* The strength of the incident shock is $p_4/p_1 = 100.0$. Other initial flow parameters are $p_1 = 1.0$, $\rho_{02} = 1.0$, $\rho_{01} = 0.1$, $u_1 = 0.0$, $\gamma_2 = 1.6667$, $\gamma_1 = 1.4$. The parameters behind the incident shock wave can be obtained via the shock relationship. The interface is initially located at $x_0 = 0.4$ while the initial position of the incident shock is at $x_{0s} = 0.3$. After

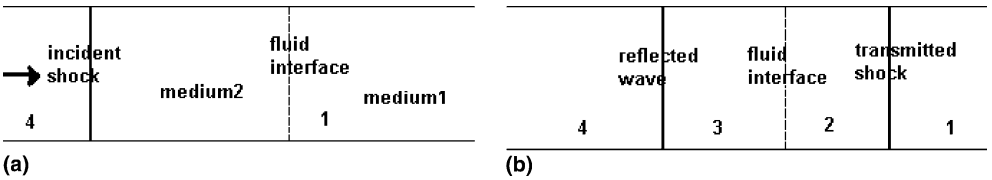


Fig. 1. (a) Before shock refraction. (b) After shock refraction.

200 time steps of computation, results obtained with the MUSCL-based original GFM are compared to the analytical solution and shown in Figs. 2(a)–(d) for the respective velocity, pressure, density and entropy. It is clear that there are discrepancies of both locations of the shock front and interface in comparison to the analysis. It may also be noted that for the density plot (Fig. 2(c)), the computed density at the higher-level magnitude indicates discernible discrepancy from the analytical result.

*Case 2 – strong shock impacting on a gas–gas interface with critical condition:* This is a specially designed case in which the initial shock strength and material densities are chosen so that the shock refraction produces no reflected wave at the interface; this is quite equivalent to shock impedance matching. The choice of these parameters also depends on the EOS used. The strength of the incident shock is maintained at $p_4/p_1 = 100.0$. Other initial flow parameters, which are chosen according to the critical condition (2.5c) to be shown in Section 2.2, are $p_1 = 1.0$, $\rho_{02} = 0.82369077$, $\rho_{01} = 1.0$, $u_1 = 0.0$, $\gamma_2 = 5/3$, $\gamma_1 = 1.2$. The

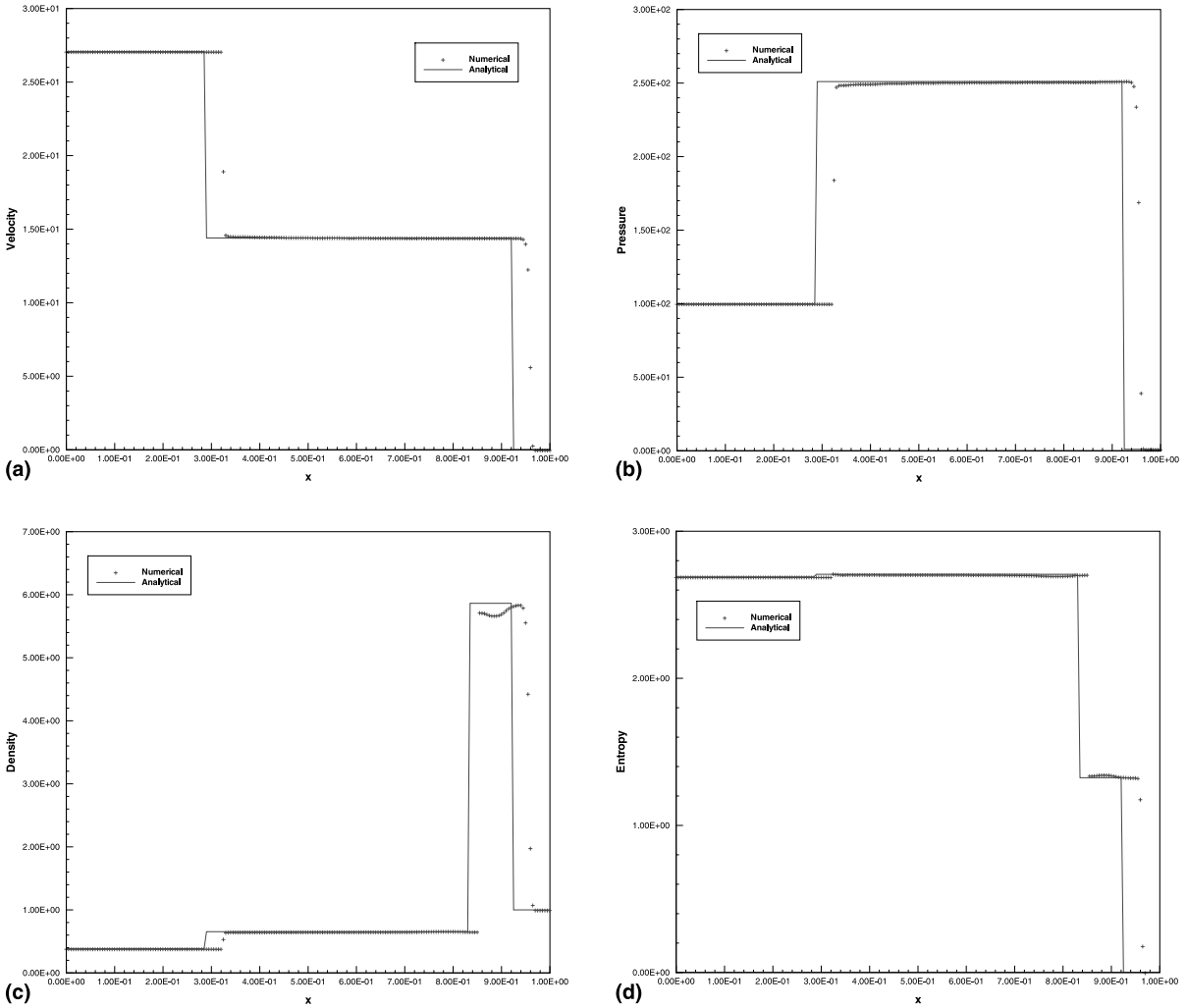


Fig. 2. (a) Velocity obtained with the original GFM and comparison to the analytical solution for Case 1. (b) Pressure obtained with the original GFM and comparison to the analytical solution for Case 1. (c) Density obtained with the original GFM and comparison to the analytical solution for Case 1. (d) Entropy obtained with the original GFM and comparison to the analytical solution for Case 1.

shock front coincides with the interface initially at $x_{0s} = x_0 = 0.2$. After 200 time steps of computation, results obtained with the MUSCL-based original GFM are shown in Figs. 3(a)–(c) for the respective velocity, pressure and density quantities. For this case, there should be no shock refraction at the interface. However, discernible non-physical hump and trough appear in the numerical results. For the density plot, there is overprediction by the numerics at the higher quantity. (It shall be shown in Section 2.2 that the non-physical hump and trough are always inherent in the original GFM.)

*Case 3 – shock impacting on a gas–water interface from air:* The strength of the incident gas shock is $p_4/p_1 = 1000.0$. Other initial flow parameters are $p_1 = 1.0$, $\rho_{02} = 1.0$, $\rho_{01} = 1000.0$, $u_1 = 0.0$, $\gamma_2 = 1.4$. For this case, a very strong shock is physically reflected back into the air. The MUSCL-based original GFM breaks down after a few time steps of computation under the employment of isentropic fixing. The internal energy fixing as suggested in [13] for the water medium is not adopted here as it is the intent to (test

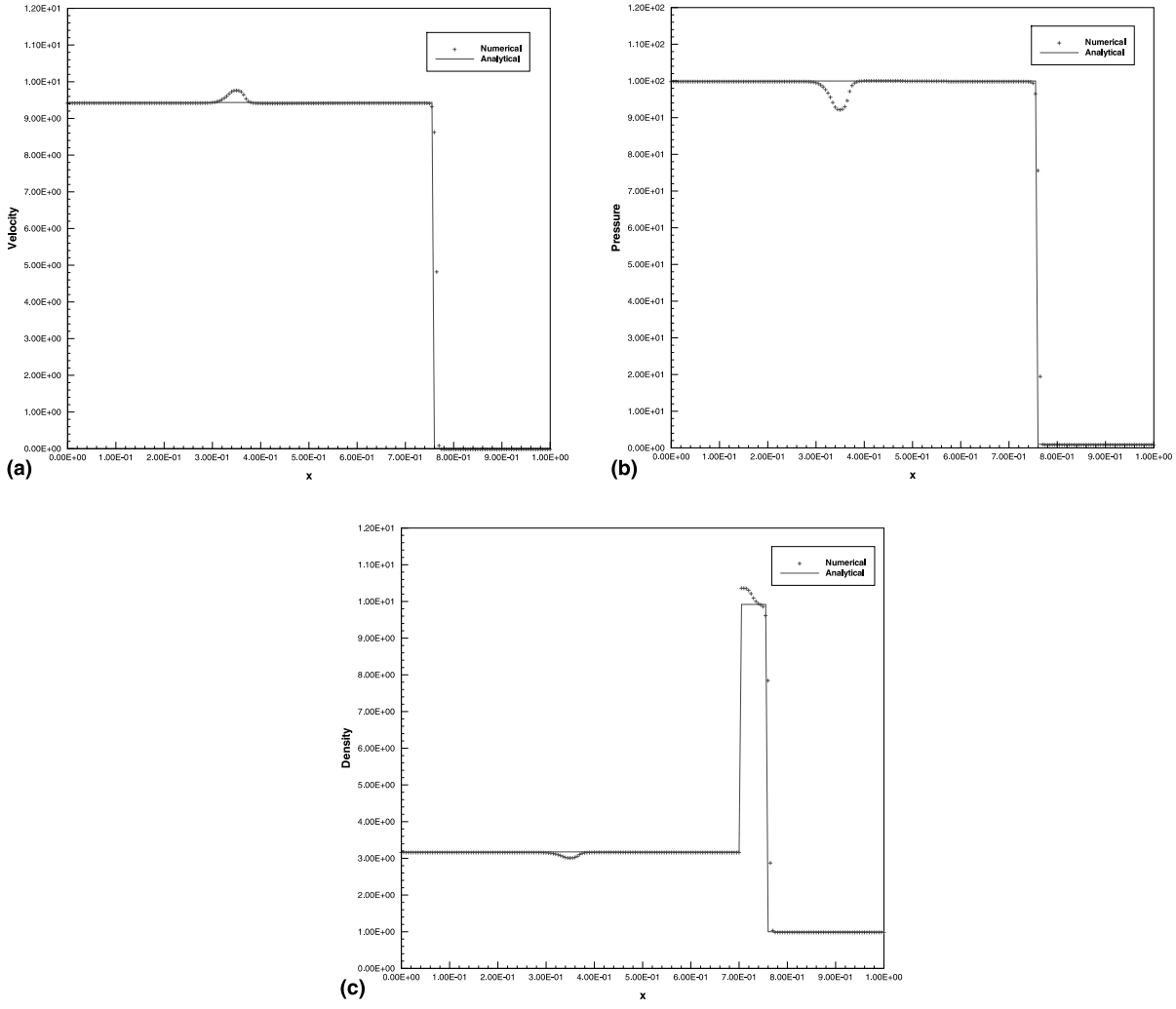


Fig. 3. (a) Velocity obtained with the original GFM and comparison to the analytical solution for Case 2. (b) Pressure obtained with the original GFM and comparison to the analytical solution for Case 2. (c) Density obtained with the original GFM and comparison to the analytical solution for Case 2.

existing one and) propose new way of constructing the ghost fluid status based on singular condition (more specifically isentropic fixing) so that the scheme can work efficiently and consistently for various EOS.

*Case 4 – underwater shock impacting on a gas–water interface:* The strength of the incident gas shock is $p_4/p_1 = 1000.0$. Other initial flow parameters are $p_1 = 1.0$, $\rho_{02} = 1000.0$, $\rho_{01} = 1.0$, $u_1 = 0.0$, $\gamma_1 = 1.4$. For this case, a very strong rarefaction wave is physically reflected back into the water. This leads to the pressure at the interface assuming a quantity that is O(100) smaller than the incident shock pressure. The MUSCL-based original GFM also breaks down after a few time steps of computation under the utilisation of isentropic fixing.

### 2.2. Shock wave interacting with material interface

To provide some insight on the difficulties encountered by the original GFM for those problems mentioned above, one has to analyze the mechanism of shock refraction at the material interface. When an incident shock wave enters from one medium into another, wave refraction occurs at the fluid interface. The incident shock is partly transmitted into the second medium and partly reflected at the fluid interface. The transmitted wave is a shock wave while the reflection may be a shock or rarefaction wave depending on medium properties, shock strength and the angle of incidence (for multidimensions). Detailed discussion on a shock interacting with a gas–gas interface can be found in [1,2]. As for an incident shock impacting on a gas–water interface, one may refer to Grove and Menikoff [10] and Liu et al. [22].

Without further details/proofs, we shall briefly list some of the important conclusions reached for the shock refraction at an interface below. Here we assume that the incident shock wave with a constant strength is traveling from medium 2 on the left towards medium 1 on the right separated by a fluid interface (see Fig. 1(a)). The interaction of the incident shock with the interface results in the transmission and reflection of the incident shock (Fig. 1(b)).

For shock wave refraction at a gas–gas interface, it can be shown the following statement holds.

*Conclusion 1:* For an incident shock wave (of constant strength) impacting on a (still) gas–gas interface, the reflected wave is a shock wave if inequality (2.5a) is satisfied, while it is a rarefaction wave if inequality (2.5b) is valid [7]. The incident shock goes through the interface without refraction if critical condition (2.5c) is held.

$$\frac{(\gamma_1 - 1)\rho_{01}}{(\gamma_2 - 1)\rho_{02}} > \frac{1 + \tau_2 p_4/p_1}{1 + \tau_1 p_4/p_1}, \tag{2.5a}$$

$$\frac{(\gamma_1 - 1)\rho_{01}}{(\gamma_2 - 1)\rho_{02}} < \frac{1 + \tau_2 p_4/p_1}{1 + \tau_1 p_4/p_1}, \tag{2.5b}$$

$$\frac{(\gamma_1 - 1)\rho_{01}}{(\gamma_2 - 1)\rho_{02}} = \frac{1 + \tau_2 p_4/p_1}{1 + \tau_1 p_4/p_1}. \tag{2.5c}$$

The pressure at the interface after shock refraction can be obtained from the following equation if the reflected wave is a shock wave [22]:

$$\sqrt{\frac{\beta_2 p_1}{\rho_{02}}}\frac{p_4/p_1 - 1}{\sqrt{1 + \tau_2 p_4/p_1}} = \sqrt{\frac{\beta_1 p_1}{\rho_{01}}}\frac{p_2/p_1 - 1}{\sqrt{1 + \tau_1 p_2/p_1}} + \sqrt{\frac{\beta_2 p_4}{\rho_4}}\frac{p_2/p_4 - 1}{\sqrt{1 + \tau_2 p_2/p_4}}, \tag{2.6a}$$

while it can be solved from

$$\sqrt{\frac{\beta_2 p_1}{\rho_{02}}}\frac{p_4/p_1-1}{\sqrt{1+\tau_2 p_4/p_1}}=\sqrt{\frac{\beta_1 p_1}{\rho_{01}}}\frac{p_2/p_1-1}{\sqrt{1+\tau_1 p_2/p_1}}+\frac{2c_4}{\gamma_2-1}\left[\left(\frac{p_3}{p_4}\right)^{(\gamma_2-1)/2\gamma_2}-1\right] \tag{2.6b}$$

if the reflected wave is a rarefaction wave, where

$$\tau_1=\frac{\gamma_1+1}{\gamma_1-1},\quad \tau_2=\frac{\gamma_2+1}{\gamma_2-1},\quad \beta_1=\frac{2}{\gamma_1-1},\quad \beta_2=\frac{2}{\gamma_2-1}. \tag{2.6c}$$

Here, $\gamma_1$ and $\gamma_2$ are the ratio of specific heats for the gas medium, $p_i$ and $u_i$ are the pressure and velocity in the "$i$th" region (Fig. 1(b)), and $\rho_{01}$ and $\rho_{02}$ are the initial gas densities before the shock impacts on the interface. $\rho_4$ is the density behind the incident shock. One solves for (2.6a) or (2.6b) for interface pressure $p_2$; exact solution can be obtained for shock refraction at a gas–gas interface for such 1D flow.

For 1D-shock refraction at a gas–water interface, we have the following conclusions.

*Conclusion 2:* Shock refraction always occurs at a gas–water interface when a shock impacts on it. The reflected wave is always a shock wave if the shock impacts on the gas–water interface from a gas side, while it is always a rarefaction wave for an underwater shock interacting with the gas–water interface (free surface) [22].

The pressure at the interface can be obtained by solving the equation:

$$\sqrt{\frac{\beta_2 p_1}{\rho_{02}}}\frac{p_4/p_1-1}{\sqrt{1+\tau_2 p_4/p_1}}=\sqrt{\frac{\bar{p}_1}{\rho_{0w}}}\sqrt{\frac{\bar{p}_2}{\bar{p}_1}-1}\sqrt{1-\left(\frac{\bar{p}_2}{\bar{p}_1}\right)^{-1/N}}+\sqrt{\frac{\beta_2 p_4}{\rho_4}}\frac{p_3/p_4-1}{\sqrt{1+\tau_2 p_3/p_4}} \tag{2.7a}$$

valid for a gas shock impacting on a free surface, while it can be obtained by solving

$$\sqrt{\frac{\bar{p}_1}{\rho_{0w}}}\sqrt{\frac{\bar{p}_4}{\bar{p}_1}-1}\sqrt{1-\left(\frac{\bar{p}_4}{\bar{p}_1}\right)^{-1/N}}=\sqrt{\frac{\beta_1 p_1}{\rho_{01}}}\frac{p_2/p_1-1}{\sqrt{1+\tau_1 p_2/p_1}}+\frac{2\bar{c}_{w4}}{N-1}\left[\left(\frac{\bar{p}_3}{\bar{p}_4}\right)^{(N-1)/2N}-1\right] \tag{2.7b}$$

for an underwater shock interacting with a free surface. Here, $\rho_{0w}$ is the initial water density. (Hereafter, the subscript "w" indicates a parameter in water.) Again, once the pressure at the interface is obtained after the shock refraction, exact solution can be obtained for such 1D flow.

Note that the above two conclusions form the basis for analysing the working of the original GFM. These conclusions are actually the results of computing the parameter range where the Riemann wave (reflected wave) curves for the gamma law (applicable to the gas medium) and Tait's EOS (applicable to the water medium) to produce the relative wave diagrams.

### 2.3. The original GFM for shock impacting on an interface

Now, we examine the satisfying of conditions (2.5a)–(2.5c) with respect to the applications of the original GFM (see Fig. 1) under the utilisation of isentropic fixing. The interface is assumed located between points $i$ and $i+1$, and the location of the incident shock coincides initially with the interface location at $x_0$ Physically, it is reckoned that the interface recovers to its normal motion instantly after a shock impacting. However, it takes a few or as many computational steps as necessary to reach this state numerically. It is within the first few steps that numerical errors can cause inaccuracy. In the first few steps, regardless of the numerical scheme used, an algorithm based on the original GFM essentially consists of solving two separate Riemann problems in the two respective single media with one-sided ghost fluid. One is in medium 2 with the initial conditions of

$$U|_{t=0} = \begin{cases} U_4, & x < x_0, \\ U_{01}^*, & x > x_0, \end{cases} \tag{2.8a}$$

and it solves from the grid point 1 on the left-end to the ghost point, say, $i+1$. The other is in medium 1 with the initial conditions of

$$U|_{t=0} = \begin{cases} U_4^*, & x < x_0, \\ U_{01}, & x > x_0, \end{cases} \tag{2.8b}$$

and it solves from the ghost point, say, $i$ to the end point on the right. Here, "*" indicates the density and thus energy have been replaced by the ghost fluid density and energy.

In the original GFM, the respective ghost fluid densities based on isentropic fixing should be

$$\rho_{01}^* = \rho_4 (p_1/p_4)^{1/\gamma_2}, \tag{2.9a}$$

$$\rho_4^* = \rho_{01} (p_4/p_1)^{1/\gamma_1}. \tag{2.9b}$$

For a single gas medium, we can draw the following conclusions from conditions (2.5a)–(2.5c).

*Conclusion 3:* For a shock impacting on a contact discontinuity in a single gas medium, there is no shock refraction, shock refraction with a reflected shock, or shock refraction with a reflected rarefaction wave if $\rho_{01}/\rho_{02} = 1$ (i.e., no longer any contact discontinuity), $\rho_{01}/\rho_{02} > 1$ or $\rho_{01}/\rho_{02} < 1$ is held, respectively. These conditions are also, respectively, true for an underwater shock impacting on a contact discontinuity in a single water medium.

The above conclusion implies that an incident shock wave always experiences shock refraction when it impacts on a contact discontinuity in single medium flow, while it may not be so in multi-medium flow. The reflection is a shock (rarefaction) wave if the incident shock impacts on an interface from the lower (higher) density side in single medium flow, while it may not be so in multi-medium flow.

The (so-called GFM) Riemann problem of (2.8a) is a shock refraction at a contact discontinuity, while the second (GFM) Riemann problem of (2.8b) is general, as the jump conditions no longer hold for the ghost fluid. It can be easily shown that

$$\frac{\rho_{01}^*}{\rho_{02}} = \frac{\rho_4}{\rho_{02}} \left(\frac{p_1}{p_4}\right)^{1/\gamma_2} = \frac{\tau_2 p_4 + p_1}{\tau_2 p_1 + p_4} \left(\frac{p_1}{p_4}\right)^{1/\gamma_2} < 1 \tag{2.10}$$

for any $p_4 > p_1$. In fact, we have following conclusions for these two Riemann problems.

*Conclusion 4:* For a shock impacting on a gas–gas interface, Riemann problem (2.8a) is a shock wave refracting at a contact discontinuity with a reflected rarefaction wave and a transmitted shock propagating in the low-pressure (ghost fluid) region. Riemann problem (2.8b) has a shock or rarefaction wave in the high-pressure (ghost fluid) region with a shock propagating in the low-pressure region; if condition (2.5a) is held, a shock wave is in the high-pressure region, while a rarefaction wave is in the high-pressure region if condition (2.5b) is satisfied.

The above statement in Conclusion 4 for Riemann problem (2.8b) can be easily verified by assuming a shock or rarefaction wave in the high-pressure region. For the shock refraction with a reflected shock, Riemann problem (2.8a) obtains a pressure magnitude at the interface lower than that for the incident shock, while Riemann problem (2.8b) provides a pressure quantity higher than that for the incident shock. Thus, Riemann problem (2.8a) works in conjunction with (2.8b) in a conflicting manner at the interface region. Moreover, condition (2.5a) is violated by Riemann problem (2.8a) due to inequality (2.10). Consequently, numerical errors are inevitably involved in the earlier time of computation. Correct magnitude of pressure and velocity, however, may still be expected subsequently due to the imposition of pressure and

velocity continuity; the second Riemann problem (2.8b) ensures an increase of pressure, and the pressure at the interface is generally of the same order as that of the incident shock for a gas medium. (This is due to the small difference of $\gamma$ among gases.) On the other hand, the conflicting behaviour of the two Riemann problems results in requiring additional time steps taken to reach the correct magnitude of pressure and velocity at the interface. If the number of time steps needed to reach the correct magnitude is very few (or not excessive), acceptable results can still be expected. This usually occurs for a less strong incident shock. In fact, when on monitoring closely the change of pressure at the interface, we found that the pressure increased incrementally from the strength of incident shock to the correct magnitude in about 10–20 steps for a milder incident shock strength and even up to 50 steps for a very strong incident shock. Therefore, the shock and interface speed cannot assume the correct value in the earlier stage. A discrepancy of shock front and interface location may, thus, be expected to be associated with the numerical solution. Due to the non-availability of reasonable isobaric value and thus the imposition of an "incorrect" isobaric value for such situations, entropy (and thus density) in the interface region may also be not correct.

Conclusion 4 also states that Riemann problems, (2.8a) and (2.8b), work in the similar manner at the interface if the reflected wave is a rarefaction wave. Condition (2.5b) is also maintained by the algorithm based on the original GFM under such a situation. Due to small difference of $\gamma$ for gases, the difference of pressure and velocity provided by the two Riemann problems is relatively not very large and the correct magnitude of pressure and velocity at the interface usually can be reached in a few time steps. Therefore, acceptable results can still be expected. On the other hand, due to the non-availability of reasonable isobaric value for the transmitted shock wave in the interface region, errors are still introduced during the earlier stage. These errors are transferred to the reflected wave through the imposition of boundary conditions. It is shown in Section 4 that a slightly widened fan may be obtained for the reflected rarefaction wave and a slight discrepancy of shock location can also occur to the transmitted shock wave when the incident shock becomes very strong. For shock tube (-like) problems, the two Riemann problems work consistently; therefore, it is not surprising that acceptable results can be obtained using the original GFM.

Conclusion 4 further implies that for a shock impacting on an interface under the critical condition as in Case 4, the transmitted shock may be captured correctly via the algorithm based on the original GFM. On the other hand, according to inequality (2.10), the critical condition of (2.5c) cannot be maintained/enforced by the algorithm based on the original GFM for the multi-medium gaseous flow. In fact, a non-physical shock refraction always occurs at the interface in such a situation during the application of the original GFM. A reflected (non-physical) trough or hump always appears in the numerical solution as shown in Figs. 3(a)–(c).

For a gas shock wave impinging on a gas–water interface, it is easy to verify that inequality (2.10) is still valid. The following conclusion, thus, can be made for the above two Riemann problems. (Now (2.8b) is a Riemann problem in the water.)

*Conclusion 5:* For a shock impacting on a gas–water interface from a gas medium, Riemann problem (2.8a) is a gas shock wave refracting at a contact discontinuity with reflected rarefaction wave and a transmitted shock propagating in the low-pressure (ghost fluid) region. Riemann problem (2.8b) consists of two (underwater) shock waves in the respective high (ghost fluid) and low-pressure regions.

Again, the two Riemann problems work in a conflicting manner at the interface. As water is less compressible, physically, a relatively very strong reflected shock wave is generated. This leads to a relatively very large jump of pressure and velocity at the interface. For the previous case of a shock impacting on a gas–gas interface with a reflected shock, interface pressure can recover incrementally to the correct magnitude, since also the magnitude is generally of the same order as the incident shock pressure and, more importantly, gases possess similar material properties. On the other hand, the sudden large jump occurring at the gas–water interface is relatively difficult to obtain via the two Riemann problems (2.8a) and (2.8b) in a few time steps. Moreover, the errors caused by the incompatibility of (2.8a) and (2.8b) at the interface can be amplified by the stiff Tait EOS in the water. As a result, the algorithm based on the original GFM can

Table 1
The pressure and velocity at the interface for various incident shock strengths for shock impacting on a gas–water interface from air

| $p4/p1(\equiv p41)$ | Pressure | | | Velocity | | |
|---|---|---|---|---|---|---|
| | Exact | RP1 | RP2 | Exact | RP1 | RP2 |
| 10.00 | 4.91E + 01 | 8.74E + 00 | 2.85E + 01 | 9.85E − 03 | 2.76E + 00 | 5.64E − 03 |
| 100.00 | 7.36E + 02 | 3.94E + 01 | 3.27E + 02 | 1.43E − 01 | 1.21E + 01 | 6.52E − 02 |
| 1000.00 | 7.51E + 03 | 1.24E + 02 | 3.32E + 03 | 1.07E + 00 | 4.86E + 01 | 5.44E − 01 |

provide inaccurate results in such a situation if isentropic fixing is employed. Table 1 shows the expected pressure and velocity at the interface for the two Riemann problems for comparison to the exact solution. Other initial non-dimensional parameters for the results shown in Table 1 are $\rho_{02} = 1.0$, $\rho_{0w} = 1000.0$, $u_1 = 0.0$ and $p_1 = 1.0$. In this table, $p41$ is the ratio of incident shock pressure $p_4$ to $p_1$, RP1 and RP2 stand for Riemann problems, (2.8a) and (2.8b), respectively. From Table 1, it can be observed that the pressure and velocity obtained by RP1 and RP2 at the interface are far away from the correct values.

Conversely, for an underwater shock impinging on a gas–water interface, we have

$$\frac{\rho_{02w}}{\rho^*_{01w}} = \frac{\rho_{02w}}{\rho_4(\bar{p}_1/\bar{p}_4)^{1/N}} = 1. \tag{2.11}$$

Thus, we have

*Conclusion 6:* For a shock impacting on a gas–water interface from water, Riemann problem (2.8a) is an underwater shock (the incident shock) passing through the interface location without shock refraction. Riemann problem (2.8b) consists of a rarefaction wave and a shock wave in the respective high (ghost fluid) and low-pressure regions.

In such a case, physically, a very strong rarefaction wave is reflected back into the water. This leads to a relatively very large sudden decrease of pressure at the interface and relatively very weak disturbance wave (transmitted shock) propagating in the gaseous medium. The pressure at the interface decreases via the gaseous Riemann problem (2.8b) in the earlier stage of computation according to the implementation of the original GFM. As mentioned, the pressure magnitude at the interface is generally of the same order as the incident shock pressure. Such a large decrease again cannot be obtained through the two single medium Riemann problems, (2.8a) and (2.8b), in a few time steps. As a result, the algorithm based on the original GFM can provide inaccurate solution under the employment of isentropic fixing. Table 2 shows the pressure and velocity at the interface for the two Riemann problems for comparison to the exact solution. (Other initial non-dimensional parameters for the results shown in Table 2 are $\rho_{01} = 1.0$, $\rho_{0w} = 1000.0$, $u_1 = 0.0$ and $p_1 = 1.0$.)

Because the algorithm based on the original GFM obtains solution essentially via computation in a single medium, the solution is somewhat related to shock refraction in a single medium. Acceptable results may thus be expected if both media possess similar properties, as analysed above. On the other hand, for shock refraction at an interface separating two media with distinctly different properties, such an algorithm

Table 2
The pressure and velocity at the interface for various incident shock strengths for shock impacting on a gas–water interface from water

| $p4/p1(\equiv p41)$ | Pressure | | | Velocity | | |
|---|---|---|---|---|---|---|
| | Exact | RP1 | RP2 | Exact | RP1 | RP2 |
| 10.00 | 1.0044 | 10.00 | 3.43E + 00 | 3.70E − 03 | 3.70E − 03 | 1.17E + 00 |
| 100.00 | 1.0487 | 100.00 | 1.25E + 01 | 4.03E − 02 | 4.03E − 02 | 2.95E + 00 |
| 1000.00 | 1.5448 | 1000.00 | 4.40E + 01 | 3.80E − 01 | 3.80E − 01 | 5.90E + 00 |

may not be able to provide reasonably accurate shock refraction; these are actually shock refraction obtained in a single-medium flow. It should be noted that medium properties play a very important role in determining the refraction pattern and interfacial conditions. Consequently, in order to employ the GFM, reasonable isobaric value and ghost fluid pressure and velocity, which are taken from the real fluid in the original GFM, have to be predicted having taken into consideration shock refraction during the shock impacting. This leads to the suggestion of a modified GFM as proposed below.

## 3. A modified GFM

As analysed above, if one wants to utilise and preserve the simplicity of the GFM, the ghost fluid status and isobaric value have to be evaluated correctly having taken into account shock–interface interaction. We can look for possible solution from the characteristic relationship and shock jump conditions. The following modification to be presented is an extension of the implicit characteristic method discussed in [21]. Overall, the proposed scheme is much simpler but still able to take into consideration the interaction of shock with the interface correctly.

### 3.1. Prediction of ghost fluid status

The two nonlinear characteristics intersecting at the interface for system (2.1) are given as

$$\frac{\mathrm{d}p_{\mathrm{I}}}{\mathrm{d}t} + \rho_{\mathrm{IL}} c_{\mathrm{IL}} \frac{\mathrm{d}u_{\mathrm{I}}}{\mathrm{d}t} = 0, \quad \text{along } \frac{\mathrm{d}x}{\mathrm{d}t} = u_{\mathrm{I}} + c_{\mathrm{IL}}, \tag{3.1a}$$

$$\frac{\mathrm{d}p_{\mathrm{I}}}{\mathrm{d}t} - \rho_{\mathrm{IR}} c_{\mathrm{IR}} \frac{\mathrm{d}u_{\mathrm{I}}}{\mathrm{d}t} = 0, \quad \text{along } \frac{\mathrm{d}x}{\mathrm{d}t} = u_{\mathrm{I}} - c_{\mathrm{IR}}, \tag{3.1b}$$

where $\rho_{\mathrm{IL}}$ ($\rho_{\mathrm{IR}}$) and $c_{\mathrm{IL}}$ ($c_{\mathrm{IR}}$) are the density and speed of sound to the left (right) of interface; $u_{\mathrm{I}}$ and $p_{\mathrm{I}}$ are the velocity and pressure at the interface. Discretising (3.1a) and (3.1b) at the interface, we obtain

$$\frac{p_{\mathrm{I}} - p_{\mathrm{IL}}}{\hat{\rho}_{\mathrm{IL}} \hat{c}_{\mathrm{IL}}} + (u_{\mathrm{I}} - u_{\mathrm{IL}}) = 0, \tag{3.2a}$$

$$\frac{p_{\mathrm{I}} - p_{\mathrm{IR}}}{\hat{\rho}_{\mathrm{IR}} \hat{c}_{\mathrm{IR}}} - (u_{\mathrm{I}} - u_{\mathrm{IR}}) = 0, \tag{3.2b}$$

where $\hat{\rho}_{\mathrm{IL}}\hat{c}_{\mathrm{IL}}$ and $\hat{\rho}_{\mathrm{IR}}\hat{c}_{\mathrm{IR}}$ are the respective approximation of $\rho_{\mathrm{IL}}c_{\mathrm{IL}}$ and $\rho_{\mathrm{IR}}c_{\mathrm{IR}}$. $u_{\mathrm{IL}}$ ($u_{\mathrm{IR}}$) and $p_{\mathrm{IL}}$ ($p_{\mathrm{IR}}$) can be evaluated along the characteristic line of $\mathrm{d}x/\mathrm{d}t = u_{\mathrm{I}} + c_{\mathrm{IL}}$ ($\mathrm{d}x/\mathrm{d}t = u_{\mathrm{I}} - c_{\mathrm{IR}}$). To apply (3.2a) and (3.2b) to a shock impacting on an interface, $\hat{\rho}_{\mathrm{IL}}\hat{c}_{\mathrm{IL}}$ and $\hat{\rho}_{\mathrm{IR}}\hat{c}_{\mathrm{IR}}$ have to be specially approximated to take into account the shock–interface interaction. As analysed above, a reflected shock is not correctly treated by the algorithm based on the original GFM. In such a situation, we have

$$\frac{p_{\mathrm{I}} - p_{\mathrm{L}}}{W_{\mathrm{L}}} + (u_{\mathrm{I}} - u_{\mathrm{L}}) = 0, \tag{3.3a}$$

$$\frac{p_{\mathrm{I}} - p_{\mathrm{R}}}{W_{\mathrm{R}}} - (u_{\mathrm{I}} - u_{\mathrm{R}}) = 0, \tag{3.3b}$$

$$W_{\mathrm{L}}^2 = \rho_{\mathrm{I}}^{\mathrm{L}} \rho_{\mathrm{L}} \frac{p_{\mathrm{I}} - p_{\mathrm{L}}}{\rho_{\mathrm{I}}^{\mathrm{L}} - \rho_{\mathrm{L}}}, \tag{3.3c}$$

$$W_{\mathrm{R}}^2 = \rho_{\mathrm{I}}^{\mathrm{R}} \rho_{\mathrm{R}} \frac{p_{\mathrm{I}} - p_{\mathrm{R}}}{\rho_{\mathrm{I}}^{\mathrm{R}} - \rho_{\mathrm{R}}} \tag{3.3d}$$

arising from the use of mass and momentum jump conditions for the respective transmitted and reflected shock. Here subscript "L" and "R" indicate the status behind the incident shock (or status ahead of the reflected shock) and the status ahead of the transmitted shock, respectively. It is easily shown that (3.3a) and (3.3b) approximate (3.2a) and (3.2b), respectively, when $p_{\mathrm{I}}$ approaches $p_{\mathrm{L}}$ and $p_{\mathrm{R}}$. Thus (3.3a)–(3.3d) approximates the characteristic system (3.1a), (3.1b) when the pressure and velocity are continuous across the interface. We use $W_{\mathrm{L}}$ and $W_{\mathrm{R}}$ to approximate $\rho_{\mathrm{IL}} c_{\mathrm{IL}}$ and $\rho_{\mathrm{IR}} c_{\mathrm{IR}}$; (3.3a) and (3.3b) are employed to predict the interface condition. Specifically, for an interface located between grid $i$ and $i+1$ at time $t = t^n$, we use the following equations to predict the interface condition (and thus the associated isobaric value) for evaluating at the next time step of $t = t^{n+1}$:

$$\frac{p_{\mathrm{I}} - p_{i-1}^n}{W_{\mathrm{L}}^n} + (u_{\mathrm{I}} - u_{i-1}^n) = 0, \tag{3.4a}$$

$$\frac{p_{\mathrm{I}} - p_{i+2}^n}{W_{\mathrm{R}}^n} - (u_{\mathrm{I}} - u_{i+2}^n) = 0, \tag{3.4b}$$

$$W_{\mathrm{L}}^{n^2} = \rho_{\mathrm{I}}^{\mathrm{L}} \rho_{i-1}^n \frac{p_{\mathrm{I}} - p_{i-1}^n}{\rho_{\mathrm{I}}^{\mathrm{L}} - \rho_{i-1}^n}, \tag{3.4c}$$

$$W_{\mathrm{R}}^{n^2} = \rho_{\mathrm{I}}^{\mathrm{R}} \rho_{i+2}^n \frac{p_{\mathrm{I}} - p_{i+1}^n}{\rho_{\mathrm{I}}^{\mathrm{R}} - \rho_{i+2}^n}, \tag{3.4d}$$

For closure of (3.4a) and (3.4b), the relationship of density and pressure must be provided. For a general EOS of (2.3), the energy jump condition can provide the relationship of density and pressure:

$$\rho_{\mathrm{I}}^{\mathrm{L}} = \frac{\left[f_2\left(\rho_{\mathrm{I}}^{\mathrm{L}}\right) + 1\right] p_{\mathrm{I}} + g_2\left(\rho_{\mathrm{I}}^{\mathrm{L}}\right) - 0.5\left(p_{\mathrm{I}} - p_{i-1}^n\right)}{\left[f_2\left(\rho_{i-1}^n\right) + 1\right] p_{i-1}^n + g_2\left(\rho_{i-1}^n\right) + 0.5\left(p_{\mathrm{I}} - p_{i-1}^n\right)} \rho_{i-1}^n, \tag{3.4e}$$

$$\rho_{\mathrm{I}}^{\mathrm{R}} = \frac{\left[f_1\left(\rho_{\mathrm{I}}^{\mathrm{R}}\right) + 1\right] p_{\mathrm{I}} + g_1\left(\rho_{\mathrm{I}}^{\mathrm{R}}\right) - 0.5\left(p_{\mathrm{I}} - p_{i+2}^n\right)}{\left[f_1\left(\rho_{i+2}^n\right) + 1\right] p_{i+2}^n + g_1\left(\rho_{i+2}^n\right) + 0.5\left(p_{\mathrm{I}} - p_{i+2}^n\right)} \rho_{i+2}^n. \tag{3.4f}$$

Eqs. (3.4e) or (3.4f) is replaced by Tait's equation if medium 2 or medium 1 is water. System (3.4a)–(3.4f) has to be solved via iteration. System (3.4a)–(3.4f) is a two-shock approximation to the Riemann problem at the interface. It provides the exact solution when a shock wave is reflected and has been shown in [21] to work very well for gas–gas or gas–water flow. It should be noted that the assumption of a rarefaction wave in the high-pressure region in a Riemann problem solver leads to wrong solution for a shock refracting with a reflected shock.

Next, we summarise the algorithm based on the modified GFM. Assume that we are solving for the flow in medium 2 (see Fig. 5 for reference, also take note of Fig. 4 for the difference between the modified GFM and the original GFM). One solves system (3.4a)–(3.4f) for prediction of the condition at the interface. Then one uses the predicted pressure and velocity as those for the ghost fluid at the ghost point $i+1$. The ghost fluid pressure and velocity at the ghost point $i+2$ can be those for the real fluid or predicted. Choosing either has no significant difference for the final results. In the present computation, the former is used. One then employs the predicted isobaric value (entropy) for medium 2 at the interface to fix the real fluid density at point $i$ to suppress the possible "overheating" and also to assign density for the ghost fluid. This is done by solving

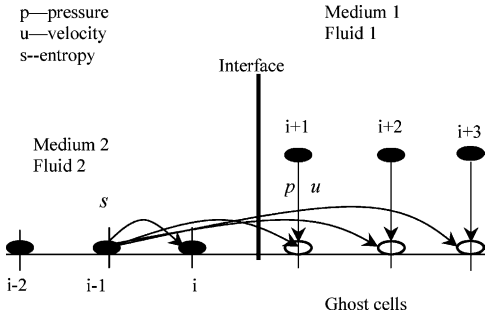


Fig. 4. Isobaric fixing for the ghost fluid method.

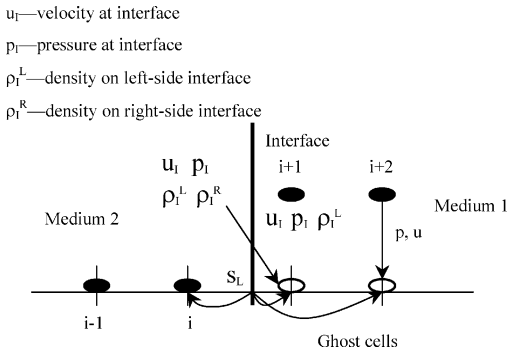


Fig. 5. Isentropic fixing for the modified ghost fluid method.

$$\frac{\mathrm{d}\rho}{\mathrm{d}p} = c^{-2} \tag{3.5a}$$

for the Mie–Gruneison EOS of (2.3) with the initial condition of $\rho(p_{\mathrm{I}}) = \rho_{\mathrm{I}}^{\mathrm{L}}$ as applied to the respective $p_i^n$, $p_{\mathrm{I}}$ and $p_{i+2}^n$. Here, $c$ is the speed of sound related to EOS (2.3) for medium 2 and can be written as

$$c^2 = -\frac{f_2' p + g'}{f_2} + \frac{(f_2+1)p + g_2}{f_2 \rho}, \tag{3.5b}$$

where "′" indicates derivative with respect to density. A similar procedure is used for computation in medium 1, where the predicted entropy at the interface for medium 1 is employed to do isobaric fixing. The rest of the procedures are the same as those for the original GFM.

Eq. (3.5a) leads to isobaric fixing with entropy. As found in [13], the isentropic fix, which is physically more natural, may not work well for gas–water flow using the original GFM. However, it works very well for the modified GFM. This also makes the present modified GFM less problem-related and more generally applicable.

Unlike the original GFM, the modified GFM calculates predicted isobaric values and ghost fluid status based on an approximate Riemann solver. This feature seems to make the modified GFM even more robust. Although good isobaric value and ghost fluid status can be predicted in the modified GFM, it can be easily shown that non-physical shock refraction still cannot be avoided for a shock impacting on a gaseous interface under *critical condition*. System (3.4a)–(3.4f) ensures accurate interface condition in the first step of such calculations under the critical situation. Thus (2.5c) is maintained by (2.8a), which also provides the

correct solution for the real fluid. On the other hand, Riemann problem (2.8b) gives rise to inaccurate solution for the real fluid. This inaccuracy is subsequently transferred via the imposition of boundary condition and thus leads to wave refraction at the interface. Unlike the original GFM, where non-physical shock refraction occurs immediately in the first step, the modified GFM causes a delayed non-physical refraction, which is expected to be a much weakened one. It is very difficult to ascertain analytically if conditions (2.5a) and (2.5b) are maintained for the modified GFM, as the predicted ghost fluid status cannot be expressed explicitly. Numerical results, however, are promising.

The computation for solving system (3.4a)–(3.4f) is cost effective as convergence is very fast even via bisection iteration. Computation for (3.5a) is minimal as the initial value predicted through system (3.4a)–(3.4f) is very close to the solution. Only a small subroutine for solving system (3.4a)–(3.4f) needs to be added to the original GFM code. Once the interface is reckoned to be (nearly) normal motion, this subroutine can be switched off. In fact, in such situation, very few iteration steps are needed for convergence.

### 3.2. Extension to multi-dimensions

Obviously, by using the present technique in the normal direction of the interface, the modified GFM can be easily implemented for multi-dimensions. Here, we briefly state its extension to multi-dimensions. First, we define a rectangular computational domain $[I_{1K}, I_{2K}] \times [J_{1K}, J_{2K}] \times [K_{1K}, K_{2K}]$ and an identification matrix $S_K$ for each medium (the $K$th medium), where $S_K(i, j, k) = 1$ if grid point (not grid cell) $(i, j, k)$ is taken by the $K$th medium, otherwise it is set to 0. We carry out the computation for each medium respectively, and denote the result by $U_K^{n+1}$ after evaluating the ghost points and doing "overheating" fixing within its computational domain. Then the final solution in the new time step is given by $U^{n+1} = \sum S_K^{n+1} U_K^{n+1}$, where $S_K^{n+1}$ is the new identification matrix of the $K$th medium, which is obtained in advance by the level set technique. One can define a computational domain for each medium that includes boundary points and grid points in the interfacial regions associated with this medium within a band of 2–4 grid points defined by $|\phi| < \varepsilon$. Here $\phi$ is the level set distance function and $\varepsilon$ is set to be about $3\min(\Delta x, \Delta y, \Delta z)$; $\Delta x$, $\Delta y$ and $\Delta z$ are spatial step sizes in the respective $x$, $y$ and $z$ directions. The way to define ghost fluid status and the calculation of "overheating" fixing within each computational domain is slightly different from that for 1D computation. Within the band of $|\phi| < \varepsilon$, if a grid point, say $(i0, j0, k0)$, is identified to be next to a fluid interface, we shall define its normal direction, $\vec{n}$, via level set function ($\vec{n} = \nabla\phi/|\nabla\phi|$). Along the normal direction, we can define a 1D Riemann problem with the initial status at the interface as

$$U|_{t=t^n} = \begin{cases} U_{n-} & \text{at one side of interface,} \\ U_{n+} & \text{at the other side of interface,} \end{cases} \tag{3.6}$$

where $U_{n-}$ and $U_{n+}$ are flow status (in two different media) at the respective spatial location of $\vec{r} = \vec{r}(i0, j0, k0) \mp 1.5\min(\Delta x, \Delta y, \Delta z)\vec{n}$, which are obtained by interpolation and the velocity is projected in the normal direction. We then solve for (3.6) using (3.4a)–(3.4f) to predict the entropy, pressure and normal velocity at the interface. If $(i0, j0, k0)$ is in real fluid, we fix the density at this point using the predicted entropy (i.e., solving (3.5a), (3.5b)), otherwise we replace the flow status with the predicted interface pressure, density and normal velocity; the tangential velocity there is defined in the same way as in [13]. For those ghost points in the band but not next to the interface, we fix the density using the closest predicted entropy and keep the pressure and velocity unchanged. There may also be ghost points in the computational domain but not within the band. For such ghost points, we only need to simply replace the density using isentropic fix with reference entropy from the real fluid, as computation to such ghost points does not affect the final result.

Now we briefly summarise the programming procedures for the modified GFM. We assume the flow variables at $t = t^n$ are known, and the following steps are taken to obtain quantities at the next time step:

1. Advance the level set function $\phi$ to the next time step and update the identification matrix $S_K^{n+1}$ for each medium over the total domain.
2. Define the computational domain $[I_{1K}, I_{2K}] \times [J_{1K}, J_{2K}] \times [K_{1K}, K_{2K}]$ for each medium.
3. Map the previous flow field in the $K$th medium computational domain to the working space; carry out the "overheating" fix for those points next to the interface in the $K$th medium (a real fluid point); replace with the predicted ghost flow status for those grid points next to the interface but not in the $K$th medium (a ghost point); fix the density with either a predicted entropy or a given reference to other ghost points inside the computational domain.
4. Use the selected single medium solver to obtain $U_K^{n+1}$ and update $U^{n+1} = U^{n+1} + S_K^{n+1} U_K^{n+1}$. ($U^{n+1}$ is initialised to zero at the beginning.)
5. Repeat steps 3 and 4 from the first medium to the last medium, and then proceed to the next time step with a new time step size.

### 3.3. On conservation error

Algorithms based on both the original GFM in [13] and the present modified GFM are non-conservative. The conservation error for the former has been discussed previously at length in [13] and shown not to be a serious problem for shock tube (-like) problems. For a strong shock impacting on an interface, however, the MUSCL-based original GFM has been shown to be unable to provide the accurate shock and interface locations over a reasonably fine mesh as discussed for Case 1 in Section 2.1. This may imply the presence of not insignificant conservation error giving rise to such a situation for the MUSCL-based original GFM. Although efforts have been made recently in constructing a conservative GFM-based algorithm [9,25], more work still awaits in implementing an efficient and fully conservative GFM-based approach for multi-dimensions. In [9], the algorithm is fairly complicated and has yet to be successfully extended to multi-dimensions. The method in [25] has been implemented in multi-dimensions using a post-processing step to redistribute the conservation error incurred in the GFM step. Whatever it is, maintaining conservation may be necessary if shock refraction occurs at the interface. This will lead to the improvement of results as shown in [25]. Besides the above-mentioned scheme of re-distributing the conservation errors in the post-processing step, it is reckoned that attention can also be directed at a fully conservative GFM-based approach and yet efficient in implementation for multi-dimensions. It is not the intent of this work to propose such a said scheme for analysis and we leave this topic to be addressed fully in our future work.

In this section, we shall examine the conservation error that occurs in the vicinity of shock impacting on the interface for both the MUSCL-based original and modified GFMs. Both overall conservation and conservation for each medium will be evaluated using Eq. (2.1) over the computational domain $[x_A, x_B]$. We denote $RHSL(t)$, $RHSR(t)$ and $RHST(t)$ as the conservation errors for the medium on the left/right side of the interface and over the whole computational domain, respectively, as follows:

$$\frac{1}{\Delta x}\left[\int_{x_A}^{x_I^{n+1}} U^{n+1}\,\mathrm{d}x - \int_{x_A}^{x_I^n} U^n\,\mathrm{d}x + \int_{t^n}^{t^{n+1}} (F_{I_L} - u_I U_{I_L} - F_A)\,\mathrm{d}t\right] = RHSL(t), \tag{3.7a}$$

$$\frac{1}{\Delta x}\left[\int_{x_I^{n+1}}^{x_B} U^{n+1}\,\mathrm{d}x - \int_{x_I^n}^{x_B} U^n\,\mathrm{d}x + \int_{t^n}^{t^{n+1}} (F_B - F_{I_R} + u_I U_{I_R})\,\mathrm{d}t\right] = RHSR(t), \tag{3.7b}$$

$$\frac{1}{\Delta x}\left[\int_{x_A}^{x_B} U^{n+1}\,\mathrm{d}x - \int_{x_A}^{x_B} U^n\,\mathrm{d}x + \int_{t^n}^{t^{n+1}} (F_B - F_A)\,\mathrm{d}t\right] = RHST(t). \tag{3.7c}$$

Here, $x_I$ denotes the interface position; $F_A$ and $F_B$ are fluxes at $x_A$ and $x_B$, respectively. $F_{I_L}$ and $F_{I_R}$ are fluxes at the respective left and right sides of the interface. Theoretically, we have

$$F_{I_L} - u_I U_{I_L} = (0, u_I, p_I)^T \tag{3.8a}$$

and

$$F_{I_R} - u_I U_{I_R} = (0, u_I, p_I)^T, \tag{3.8b}$$

and the summing of (3.7a) and (3.7b) leads to (3.7c). The conservation property requires that (3.7a), (3.7b) and thus (3.7c) are always equal to zero. Most of the Eulerian method for multi-medium flow maintains (3.7c) but not for (3.7a) and (3.7b) due to numerical smearing at the interface. By considering $RHSL(t)$, $RHSR(t)$ and $RHST(t)$ at each time step, the conservation errors arising from the numerics pertinent to the numerical method employed can be evaluated. As analysed above, the algorithm based on the original GFM obtains solution essentially via computation in the single medium flow and Riemann problems (2.8a) and (2.8b) are unable to provide identical pressure and velocity at the interface during the shock impacting; the equality between (3.8a) and (3.8b), thus, cannot be maintained in the computation. Consequently, there is no conservation for the respective medium or over the whole computation domain, and large conservation error can occur. On the other hand, the modified GFM with predicted interface status can approximate the correct interfacial pressure and velocity, with the conservation error for the latter suppressed to some extent. Figs. 6(a)–(c) show the conservation errors of mass, momentum and energy for both MUSCL-based original and modified GFMs in the first 100 time steps of computation carried out for Case 1 of Section 2.1 starting from the shock impacting. (Further discussion and detailed results of the modified GFM are given in Section 4.2.) In these figures, MGFM stands for the modified GFM, "left-medium" and "right-medium" indicate the conservation errors for the respective media on the left and right sides of the interface, "total" indicates the conservation error over the whole computational domain. From these figures, it is clear that very large errors incur for the MUSCL-based original GFM in the first 10 steps for this specific case, while these are suppressed very well by the MUSCL-based modified GFM. After about 20 time-step computation, negligible (new) conservation errors are brought into numerical results for both MUSCL-based original and modified GFMs. This strongly suggests that most of conservation errors occur in the earlier stage of shock impacting.

## 4. Applications

Several tests will be implemented for both the original GFM and the modified GFM. For problems related to shock impacting on an interface, the strength of the incident shock is assumed to be very high. These problems, which are often encountered in explosions in air or shallow water, are very trying for the algorithm based on the original GFM. It is surmised that these problems may also be very challenging for other numerical methods dealing in multi-medium flows. All the computations below are done using second order MUSCL with CFL = 0.9 for both the original and modified GFMs with 201 uniform mesh points in domain $[0, 1]$ for 1D calculations unless otherwise noted. Isentropic fixing (3.5a), (3.5b) is employed for both the original and modified GFMs. The interface is captured using the Level-Set technique as presented in [21] with re-initialisation. Although the theoretical analysis carried out and conclusions made in the present work with regard to the original GFM are independent of the numerical scheme used, it may be noted that the extent and magnitude of numerical accuracy are likely dependent on the actual numerical solver employed.

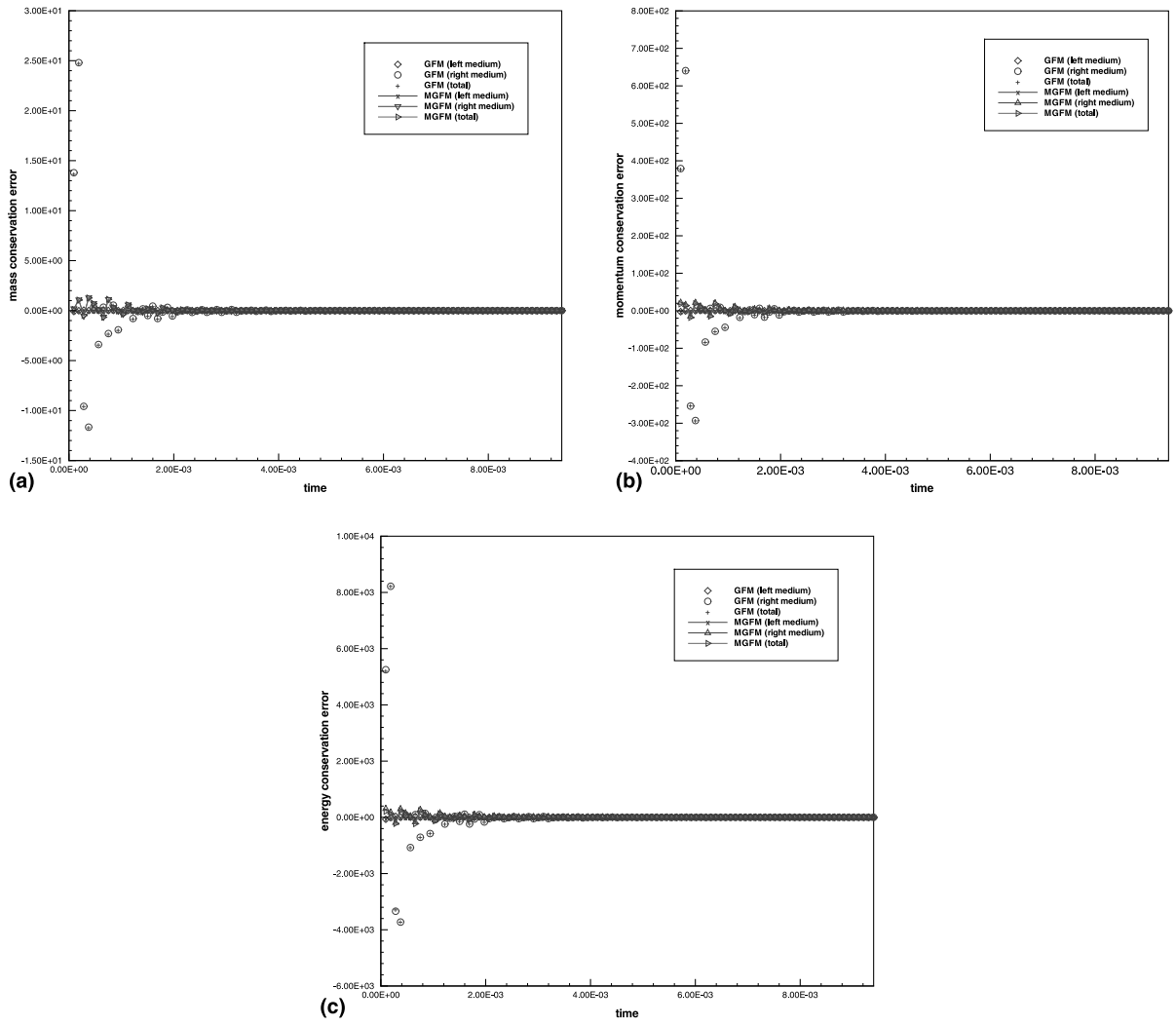


Fig. 6. (a) Comparison of mass conservation error for Case 1 between the original GFM and the modified GFM (MGFM). (b) Comparison of momentum conservation error for Case 1 between the original GFM and the modified GFM (MGFM). (c) Comparison of energy conservation error for Case 1 between the original GFM and the modified GFM (MGFM).

### *4.1. Shock tube (-like) problems*

Three problems will be simulated. These are gas shock tube problem, gas–water shock tube problem and 1D-plane explosion in water. This is to demonstrate that the MUSCL-based modified GFM works well for those kinds of problems where the MUSCL-based original GFM is also valid. The initial condition is

$$U|_{t=0} = \begin{cases} U_{\mathrm{H}}, & x < x_0, \\ U_{\mathrm{L}}, & x > x_0. \end{cases} \tag{4.1}$$

Hereafter, subscripts "H" and "L" indicate the initial statuses of the high and low-pressure region, respectively; $x_0$ is the initial interface position. Results between the two methods look very similar and compared well to the analysis; the results of the MUSCL-based original GFM are not depicted here.

*Gas-shock tube problem (problem 1):* The initial flow parameters on both sides of the interface are $p_H = 10.0$, $p_L = 1.0$, $\rho_H = 2.0$, $\rho_L = 1.0$, $u_H = u_L = 0.0$, $\gamma_H = \gamma_L = 1.4$. The interface is initially located at $x_0 = 0.5$. After 100 time steps of computation, results given by the modified GFM are compared to the analytical solution, and shown in Figs. 7(a)–(c) for the respective velocity, pressure and density. The comparison is reasonably good.

*Gas–water shock tube problem (problem 2):* The initial high-pressure region is located on the gas side. The initial flow parameters on both sides of the interface are $p_H = 8000.0$, $p_L = 1.0$, $\rho_H = 1.27$, $\rho_L = 1.0$, $u_H = u_L = 0.0$, $\gamma_H = 1.4$. Tait's EOS is employed for the water. The interface is initially located at $x_0 = 0.4$. After 100 time steps of computation, results obtained using the modified GFM are compared to the analytical solution and shown in Figs. 8(a)–(c) for the respective velocity, pressure and density. The

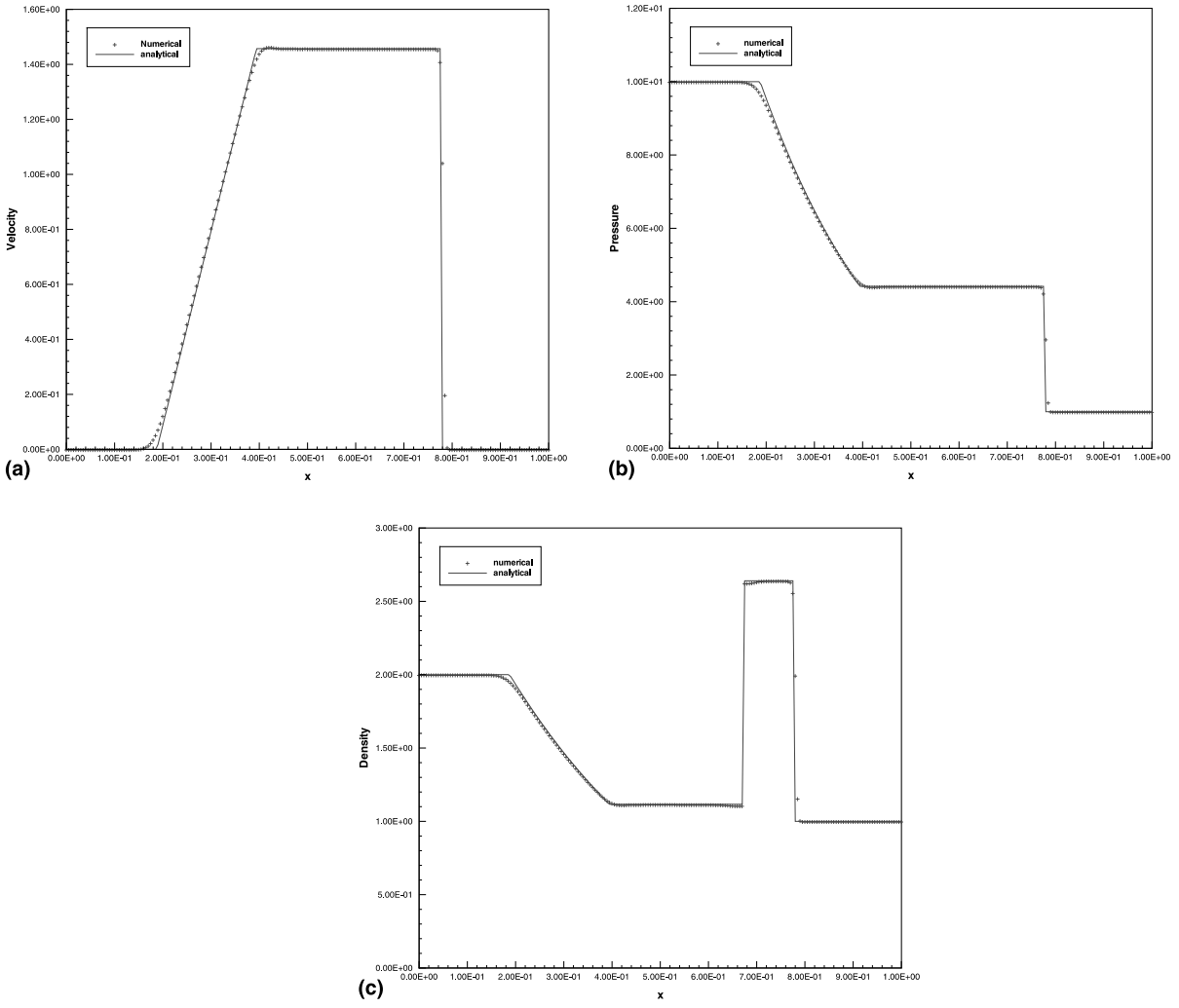


Fig. 7. (a) Velocity obtained with the modified GFM and comparison to the analytical solution for problem 1. (b) Pressure obtained with the modified GFM and comparison to the analytical solution for problem 1. (c) Density obtained with the modified GFM and comparison to the analytical solution for problem 1.

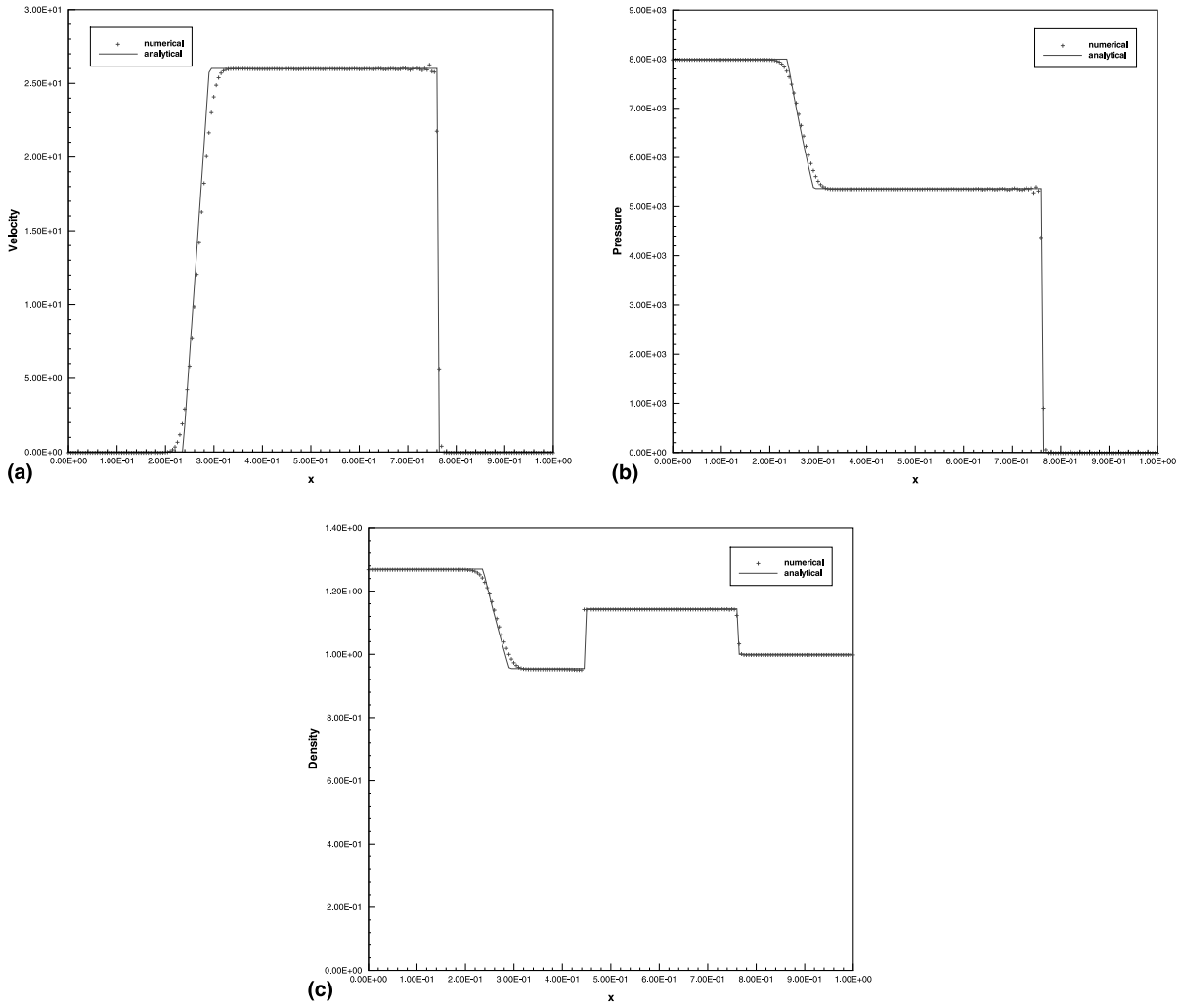


Fig. 8. (a) Velocity obtained with the modified GFM and comparison to the analytical solution for problem 2. (b) Pressure obtained with the modified GFM and comparison to the analytical solution for problem 2. (c) Density obtained with the modified GFM and comparison to the analytical solution for problem 2.

marginally very small oscillation discerned immediately behind the shock wave is well contained and which also appears in the results of the MUSCL-based original GFM. In fact, results between the modified and original GFM look identical in plots.

*1D-plane explosion in water (problem 3):* This problem is the example 4 given in [13]. Explosive with JWL EOS is assumed to drive the water with the initial flow parameters of $p_{\mathrm{H}} = 7.81 \times 10^9$ Pa, $p_{\mathrm{L}} = 1.0 \times 10^5$ Pa, $\rho_{\mathrm{H}} = 1630$ kg/m$^3$, $\rho_{\mathrm{L}} = 1000.0$ kg/m$^3$, $u_{\mathrm{H}} = u_{\mathrm{L}} = 0.0$ m/s. Tait's EOS is used for the water. The computational domain is $[0, 4m]$ with 201 uniform grid points. The interface is initially located at $x_0 = 2.0$ m. After 100 time steps of computation, results obtained with the modified GFM are compared to the analytical solution and shown in Figs. 9(a)–(c) for the respective velocity, pressure and density. Again, there is very close similarity between the MUSCL-based modified and original GFMs.

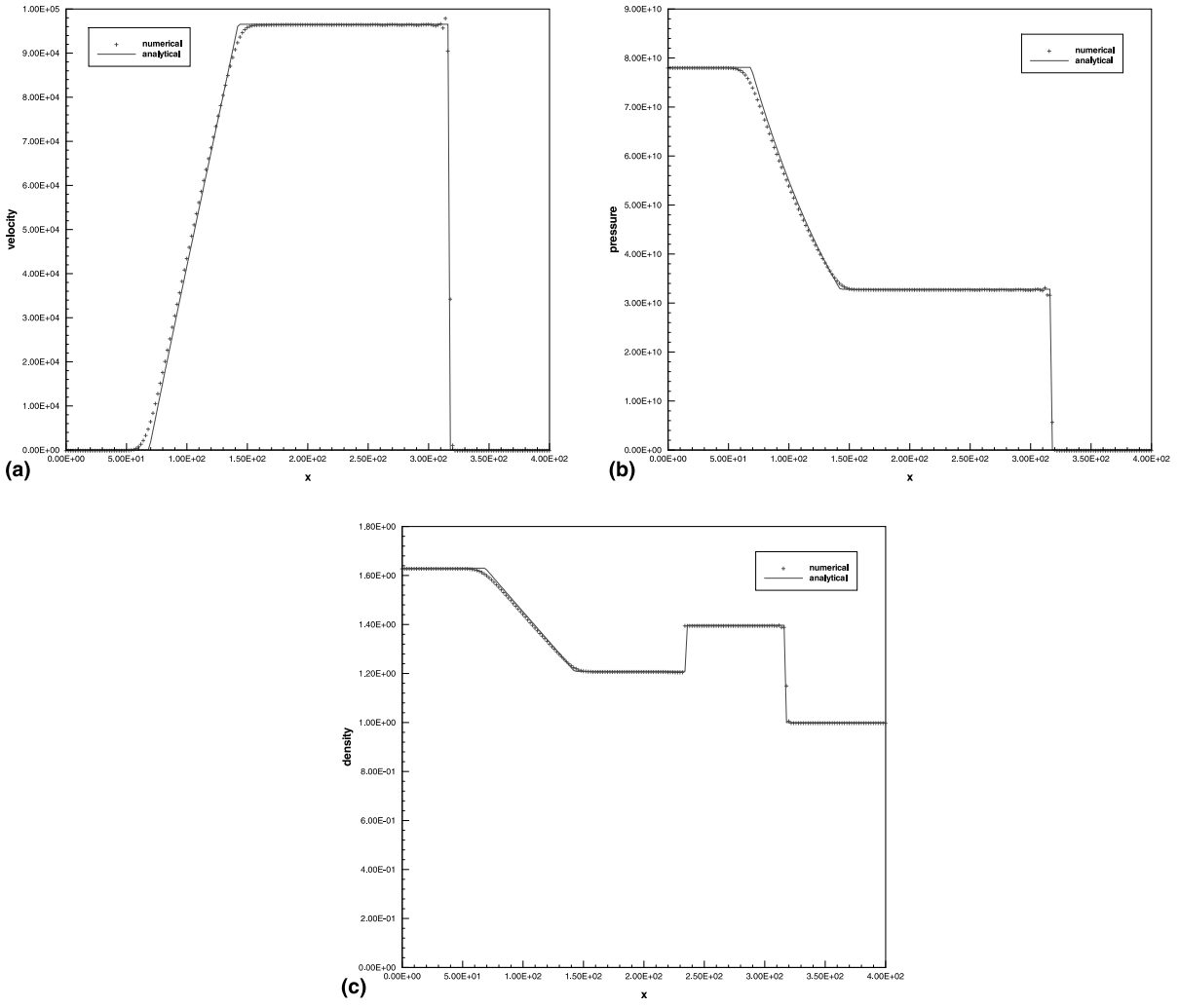


Fig. 9. (a) Velocity obtained with the modified GFM and comparison to the analytical solution for problem 3. (b) Pressure obtained with the modified GFM and comparison to the analytical solution for problem 3. (c) Density obtained with the modified GFM and comparison to the analytical solution for problem 3.

### 4.2. Shock impacting on a gas–gas interface

Three situations as analysed in Section 2.3 will be simulated depending on the strength of incident shock and material properties. The general initial condition is as given in (2.4).

*Shock refraction with reflected rarefaction wave (problem 4):* The strength of the incident shock is $p_4/p_1(\equiv p41) = 100.0$. Other initial flow parameters are $p_1 = 1.0$, $\rho_{02} = 1.0$, $\rho_{01} = 0.1$, $u_1 = 0.0$, $\gamma_2 = 1.6667$, $\gamma_1 = 1.4$. The interface is initially located at $x_0 = 0.2$. The initial position of the incident shock front is also assumed at $x_{0s} = 0.2$. After 200 time steps of computation, results obtained with the MUSCL-based original GFM are compared to the analytical solution and shown in Figs. 10(a)–(c) for the respective velocity, pressure and density. The corresponding results of the modified GFM are shown in Figs. 11(a)–(c). The MUSCL-based original GFM, just as we have analysed in Section 2.3, performed very well for this problem

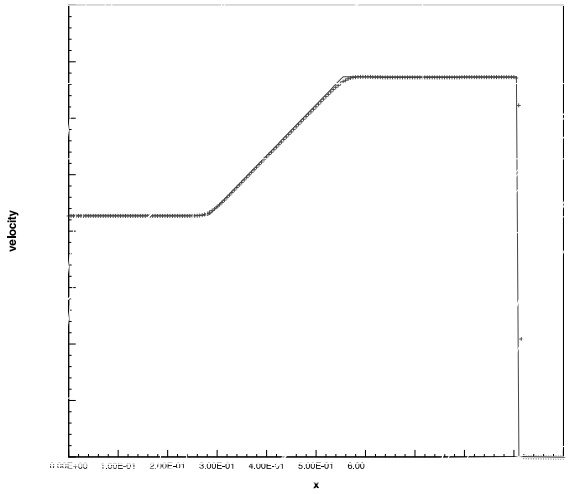


with a moderate strength of incident shock wave. Next, we increase the strength of incident shock wave to 1000.0 (i.e., $M_1 = 1000.0$) and all other initial conditions remain unchanged. The results of the MUSCL-based original GFM are shown in Figs. 12(a)–(c) for the respective pressure, density and entropy. Discrepancies with analytical solution appear. There is a discrepancy of interfacial location and transmitted shock position. Not to mention is the underestimated computed entropy, which leads to overestimated density ("underheating") next to the interface for medium 1 as shown in Figs. 12(b) and (c), respectively. This is attributed to the imposition of incorrect entropy fixing for the transmitted shock during the shock–interface interaction. Under such a situation, the correct isobaric value cannot be provided via the local flow information. To obtain an acceptable isobaric value, one has to solve an exact or approximate Riemann problem. The isentropic fixing in the original GFM causes the earlier formation of transmitted shock with inaccurate entropy. Although the transmitted shock wave has been restored to a normal shock wave

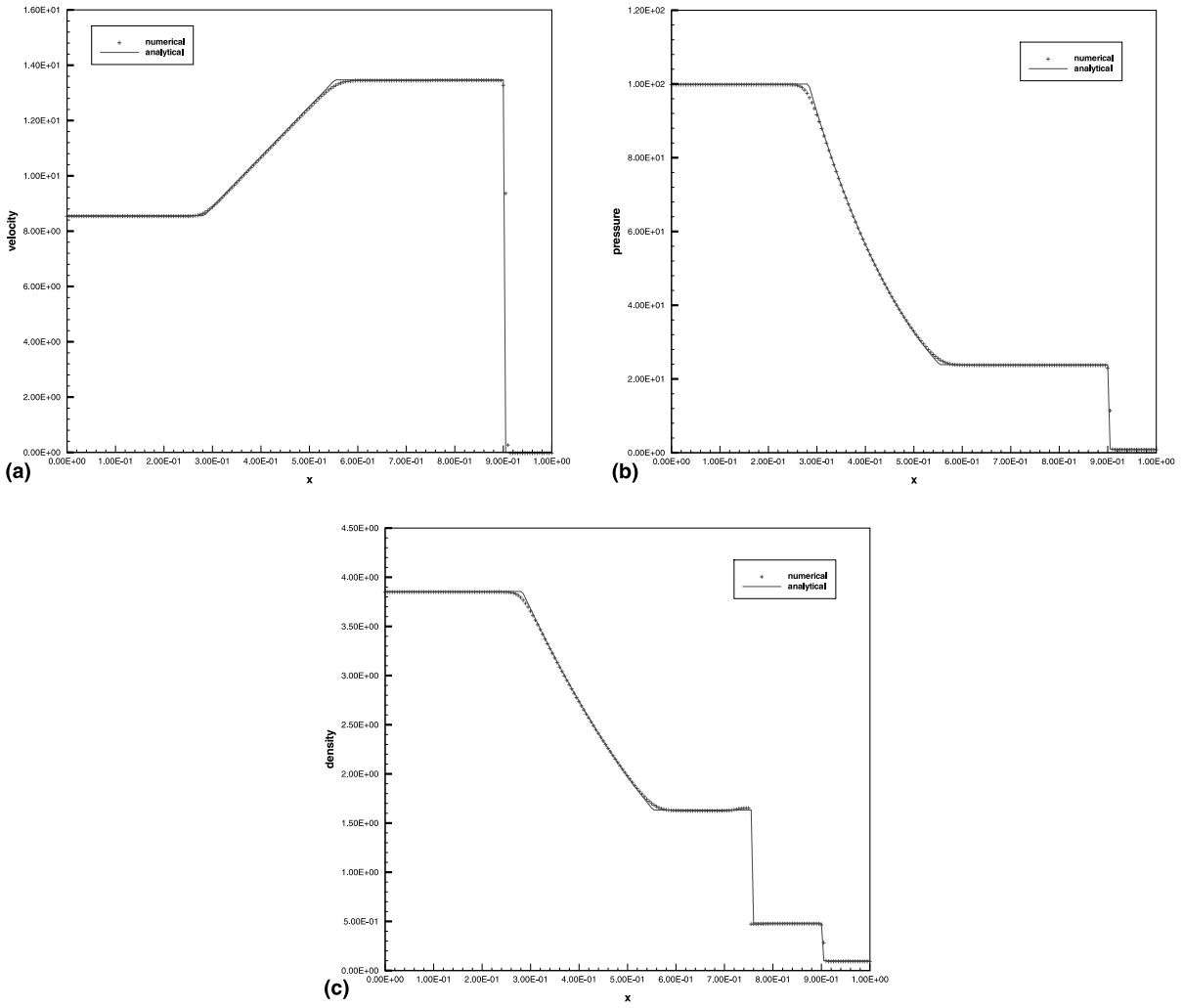


Fig. 11. (a) Velocity obtained with the modified GFM and comparison to the analytical solution for problem 4. (b) Pressure obtained with the modified GFM and comparison to the analytical solution for problem 4. (c) Density obtained with the modified GFM and comparison to the analytical solution for problem 4.

subsequently when it propagates away from the interface, the error is distributed and transferred to medium 2 through the boundary condition, leading to a widened rarefaction wave fan besides the inaccurate shock position (Figs. 12(a) and (b)). Results of the modified GFM are shown in Figs. 13(a)–(c). All major discrepancies appearing in Figs. 12(a)–(c) for the original GFM do not show up.

*Shock refraction with reflected shock wave (problem 5 – Case 1):* The initial flow conditions are similar to Case 1 of Section 2.1. The initial position of incident shock is assumed to coincide with the interface location (i.e., $x_{0s} = x_0 = 0.3$.). After 350 time steps of computation, the results of modified GFM are shown in Figs. 14(a)–(d). (The MUSCL-based original GFM results are shown in Figs. 2(a)–(d) with $x_{0s} = 0.3$ and $x_0 = 0.4$ at 200 time steps.) With the increase or imposition of sufficiently large incident shock strength, the results by the MUSCL-based original GFM become unacceptable. This lends supports to the earlier discussion that the inaccuracy manifested in Figs. 2(a)–(d) is inherent in the original GFM. As also discussed,

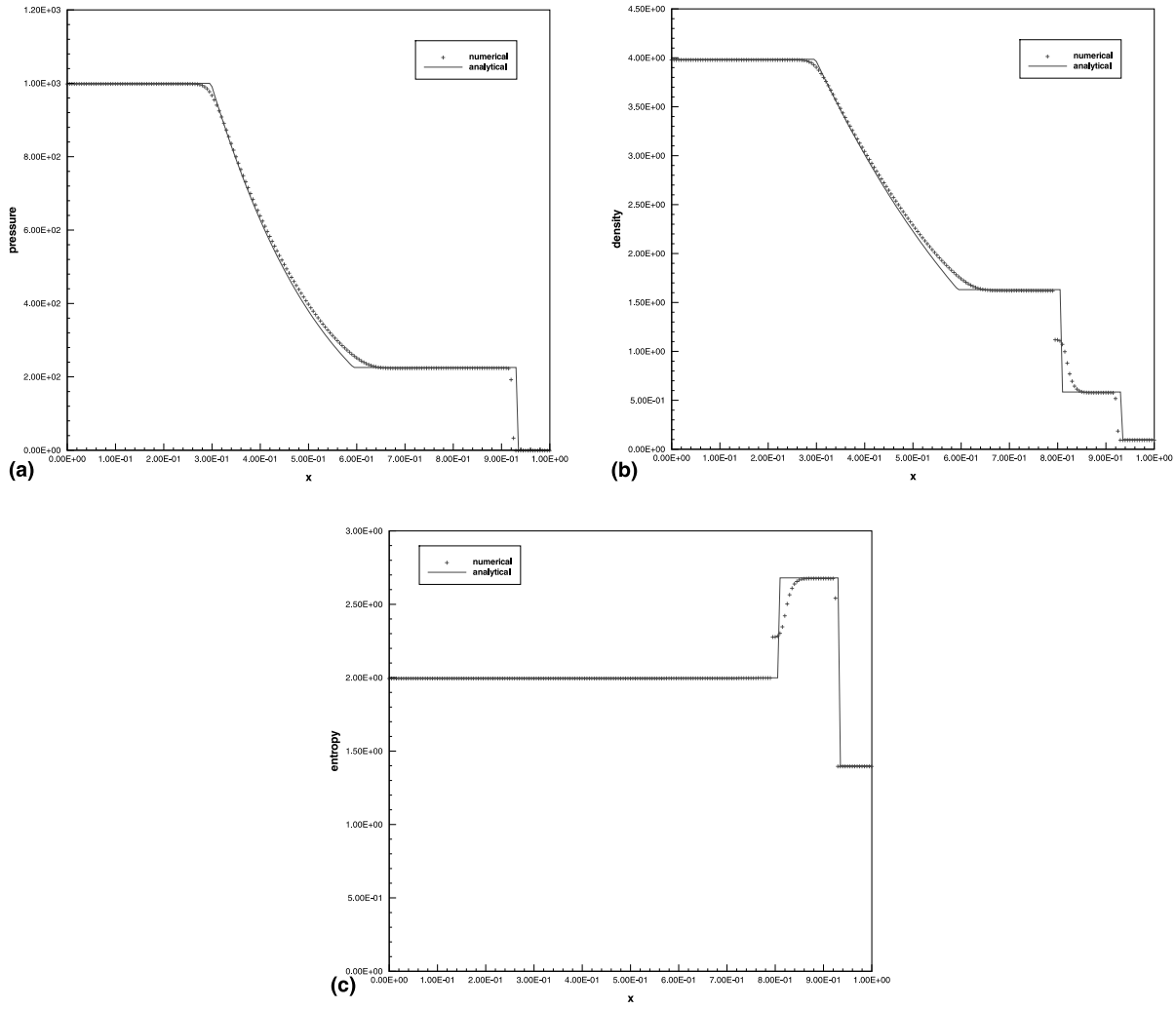


Fig. 12. (a) Pressure obtained with the original GFM and comparison to the analytical solution for problem 4 with $p41 = 1000.0$. (b) Density obtained with the original GFM and comparison to the analytical solution for problem 4 with $p41 = 1000.0$. (c) Entropy obtained with the original GFM and comparison to the analytical solution for problem 4 with $P41 = 1000.0$.

the influence of material properties during the wave interaction with interface must be taken into account. Primarily due to the isobaric fixing of the incorrect value, the inaccuracy of entropy in the interfacial region is clearly exhibited in Fig. 2(d). All undesirable or incorrect features appearing in Figs. 2(a)–(d) do not occur for the modified GFM (Figs. 14(a)–(d)).

*Shock refraction with critical condition (problem 6 – Case 2):* The initial condition for this computation is identical to that for Case 2 in Section 2.1. Results obtained using the MUSCL-based original GFM are given in Figs. 3(a)–(c). After 200 time steps of computation, the results of modified GFM are shown in Figs. 15(a)–(c). As observed, the transmitted shock can be captured very well under such (critical) situation. However, a non-physical shock refraction cannot be avoided by either GFM, since the solution is calculated essentially in the single medium flow, which leads to the violation of critical condition (2.5c). Since the isobaric value is predicted correctly and the ghost fluid status is replaced by predicted interfacial status, the


...ysical hump and

...*Case 3)*: This test is a gas shock refracting at the ... similar to Case 3 of Section 2.1. The interface is ... ...tion of inci... ...ock is also assumed at $x_{0s} = 0.5$. After 350 time ... ...d with the modifie... ...M are shown in Figs. 16(a)–(c) for the respective ... ...he pressure behind the re... ...l shock wave is 7507.0, which is about 7.5 times

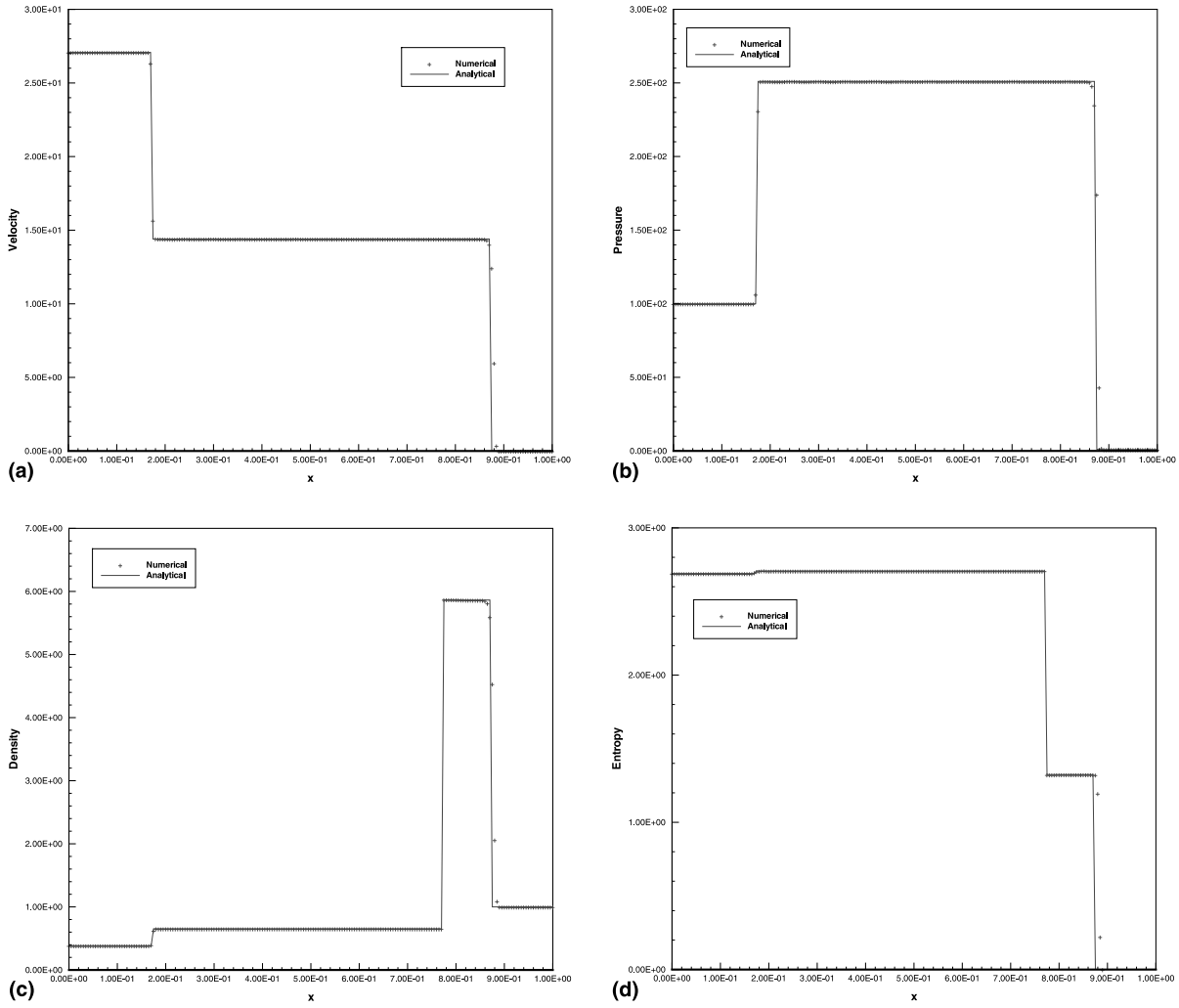


Fig. 14. (a) Velocity obtained with the modified GFM and comparison to the analytical solution for problem 5 (Case 1). (b) Pressure obtained with the modified GFM and comparison to the analytical solution for problem 5 (Case 1). (c) Density obtained with the modified GFM and comparison to the analytical solution for problem 5 (Case 1). (d) Entropy obtained with the modified GFM and comparison to the analytical solution for problem 5 (Case 1).

higher than the incident shock pressure. Such a great sudden increase usually spells potential problem. The MUSCL-based original GFM with isentropic fixing for both the gas and water media breaks down after a few time steps of computation. The modified GFM works well and concurs with the analytical solution. It may be added that an even higher incident shock strength was computed and there is good agreement with analysis.

*Shock refraction with reflected rarefaction wave (problem 8 – Case 4):* This situation occurs for an underwater shock refracting at a free (gas–water) surface. The initial conditions are the same as Case 4 of Section 2.1. The interface is initially located at $x_0 = 0.7$. The initial position of incident shock is also assumed to be at $x_{0s} = 0.7$. After 150 time steps of computation, results obtained with the modified GFM are shown in Figs. 17(a)–(c) for the respective velocity, pressure and density. It is observed that a relatively very weak transmitted shock propagates in the gas and yet is successfully captured by the scheme. The pressure behind the transmitted shock wave is about 1.55 or about 700.0 times lower than the incident shock

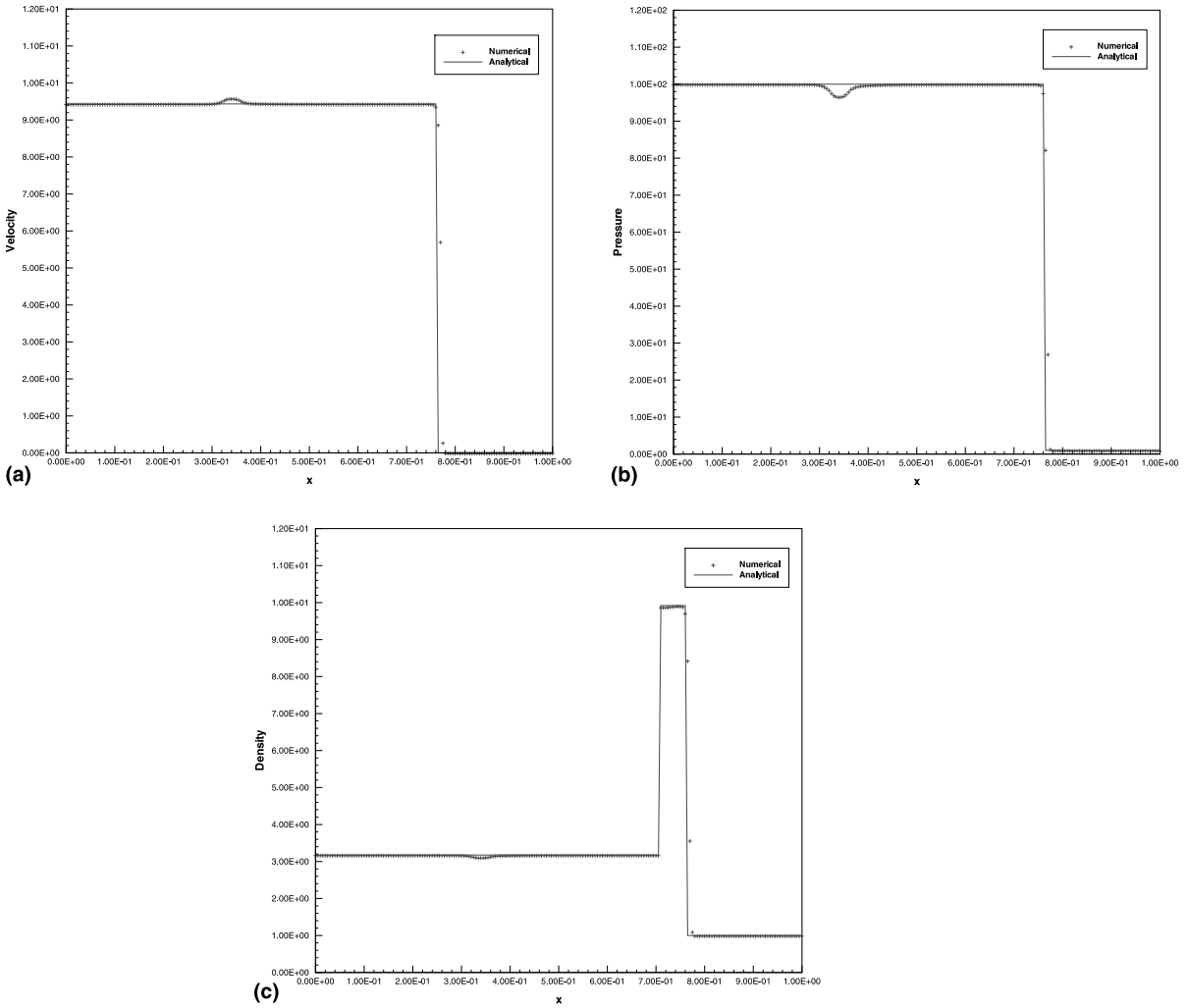


Fig. 15. (a) Velocity obtained with the modified GFM and comparison to the analytical solution for problem 6 (Case 2). (b) Pressure obtained with the modified GFM and comparison to the analytical solution for problem 6 (Case 2). (c) Density obtained with the modified GFM and comparison to the analytical solution for problem 6 (Case 2).

pressure. Such a great sudden decrease causes difficulty for the MUSCL-based original GFM using only isentropic fixing. In fact, the MUSCL-based original GFM either breaks down for this kind of problems or provides unacceptable solution in the water region. (In [13], to avoid this difficulty for the gas–water problem, internal energy fixing is suggested for the water medium.) The modified GFM with isentropic fixing applied for both media works well and the results concur with analysis.

### *4.4. 2D applications*

The intent of this section is to show the applicability of the extension of the modified GFM to higher dimensions. Generally, the results obtained are comparable to previous works and able to capture all the important features successfully.

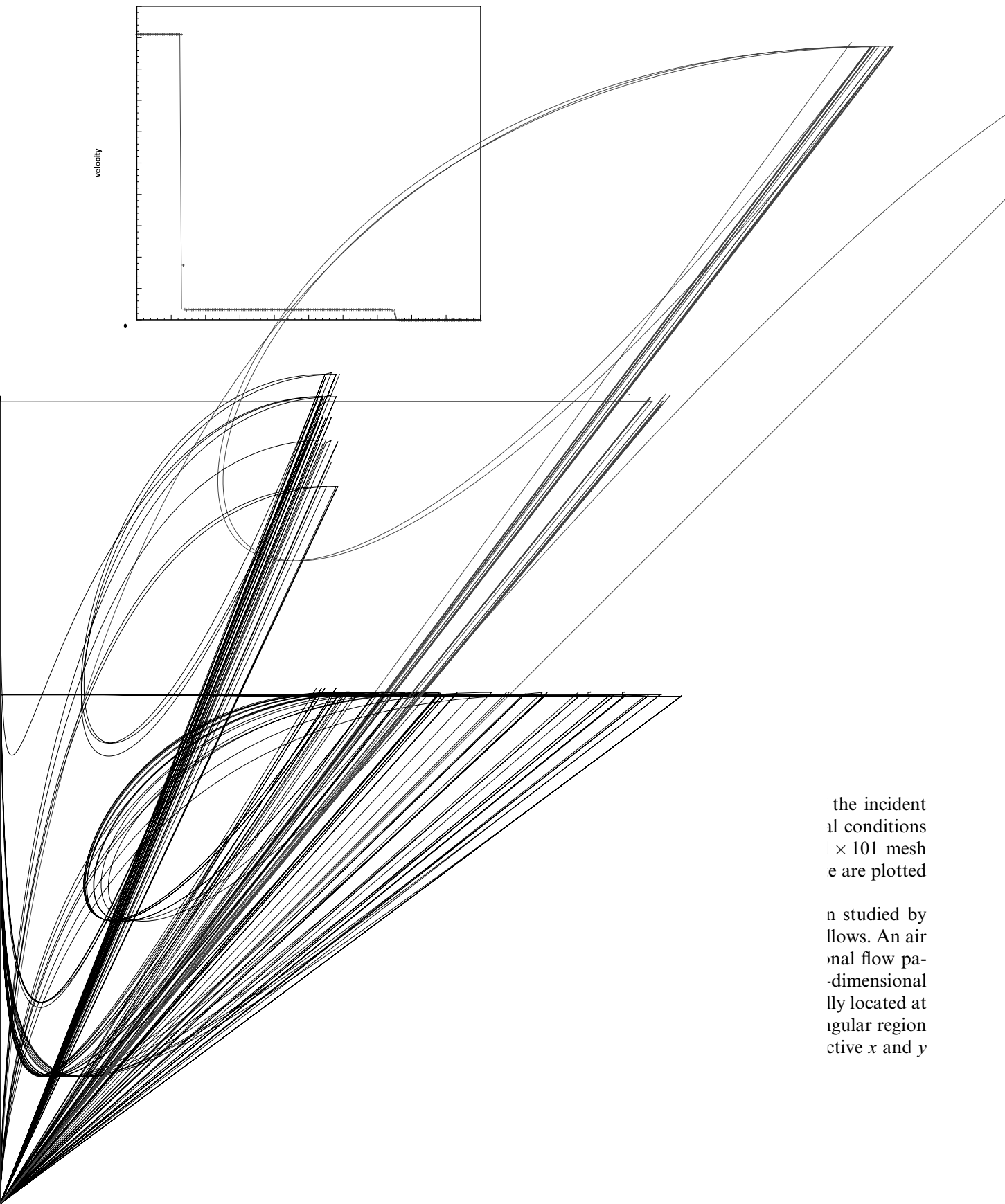


the incident
ıl conditions
× 101 mesh
e are plotted

n studied by
llows. An air
ɔnal flow pa-
-dimensional
lly located at
ıgular region
ctive $x$ and $y$

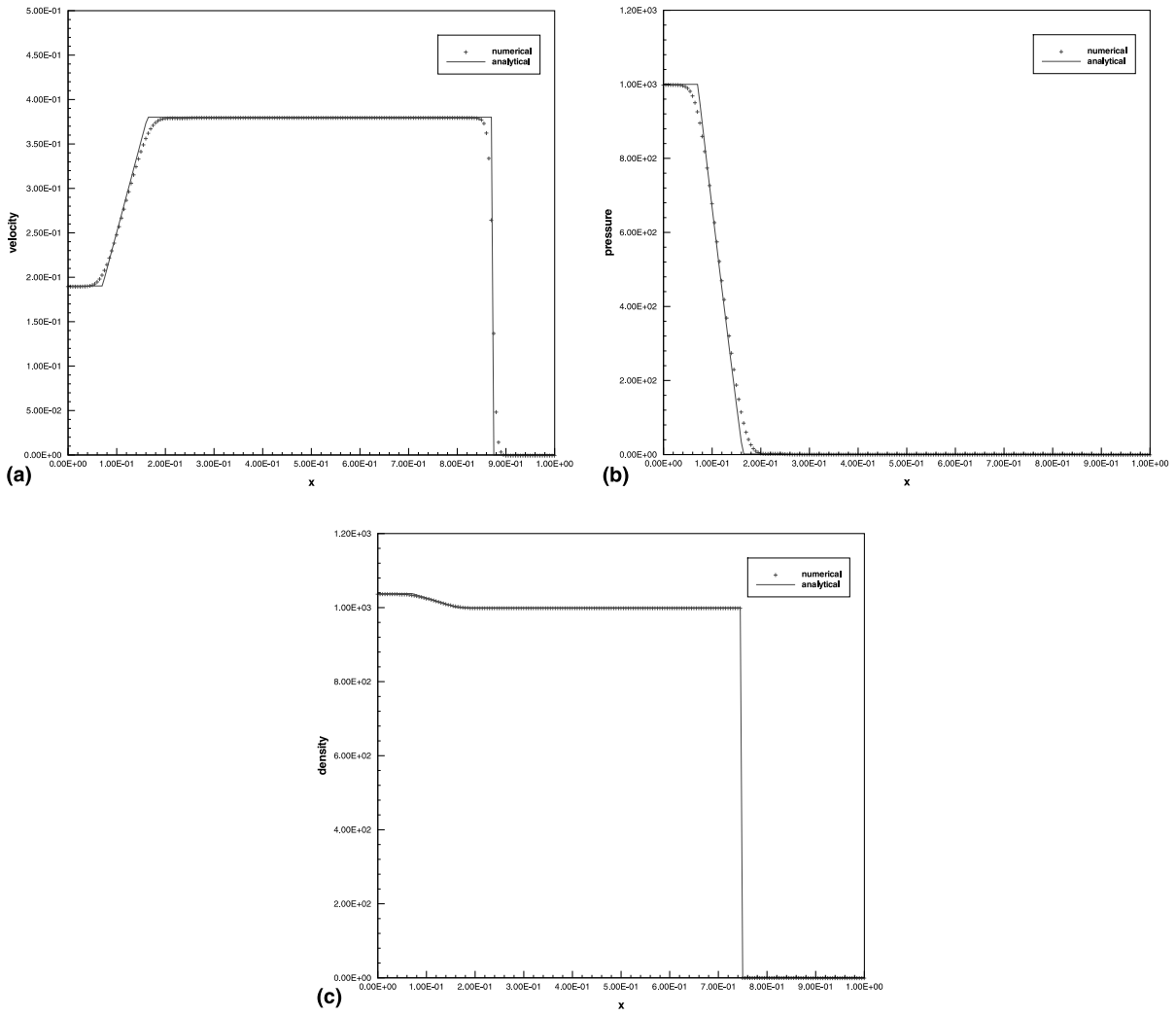


Fig. 17. (a) Velocity obtained with the modified GFM and comparison to the analytical solution for problem 8 (Case 4). (b) Pressure obtained with the modified GFM and comparison to the analytical solution for problem 8 (Case 4). (c) Density obtained with the modified GFM and comparison to the analytical solution for problem 8 (Case 4).

directions. CFL is taken to be 0.45. The re-initialisation of level-set function is carried out once every 10 steps. Fairly complex physics occur in this model. In the earlier stage, the shock refraction on the bubble surface is regular initially but transits into an irregular type after the incident shock past over a critical angle [10,22]. The detailed physical analysis can be found in [22] especially for the earlier stage. Figs. 19(a) and (b) show the typical density contours at the respective 100 and 200 time-step computation. All the main features of the flow are successfully captured and comparable to [22].

## 5. Conclusions

In this paper, a modified GFM was developed to overcome the difficulties encountered by the original GFM as applied to a strong shock impacting on a material interface. The plausible causes for the

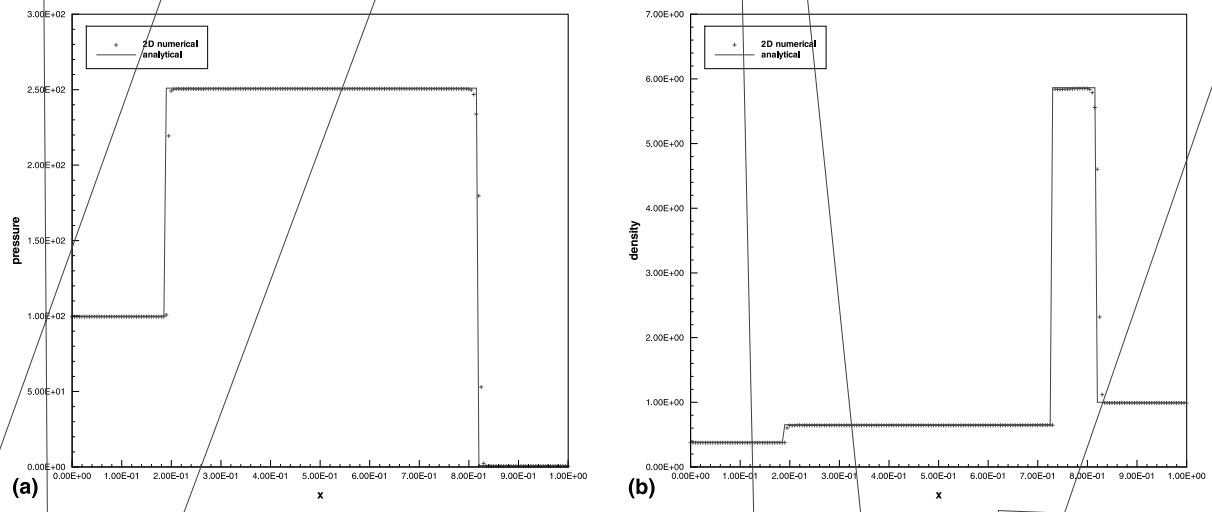


Fig. 18. (a) Pressure obtained with the modified 2D GFM for problem 9 (same as problem 5, Case 1). (b) Density obtained with the modified 2D GFM and comparison to the analytical solution for problem 9 (same as problem 5, Case 1).

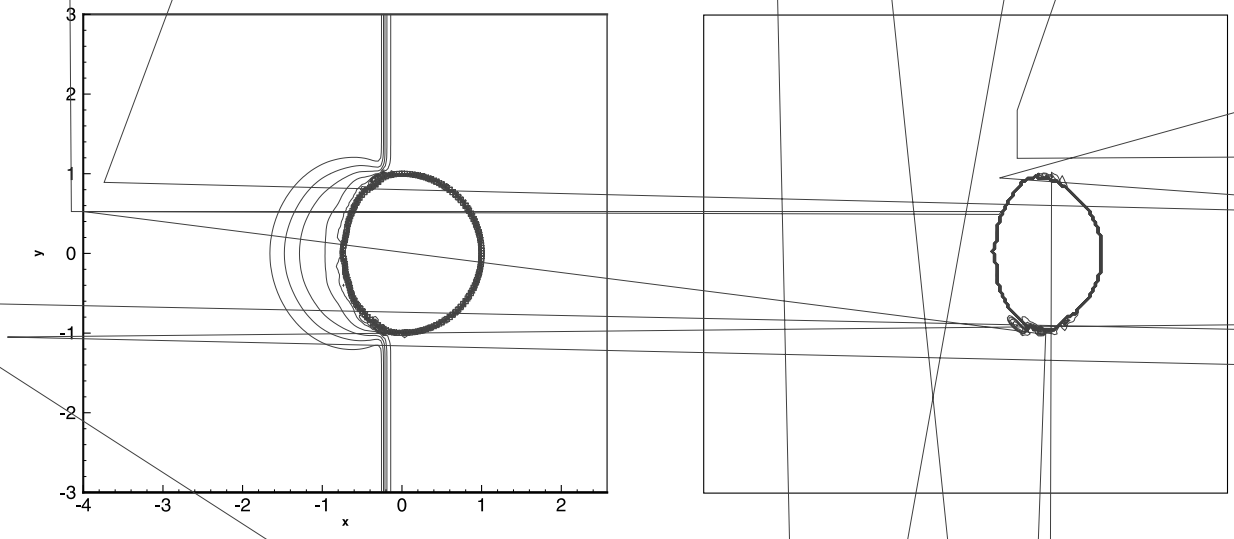


inapplicability of the original GFM for such said simulations were analysed and discussed in great detail. A modified GFM based on isentropic fixing with predicted entropy and ghost fluid status has been suggested which can be applied consistently and efficiently to various types of EOS. Numerical tests have shown that the modified GFM is applicable to both very strong and not-so-strong shock impacting and interacting with a material interface. The extension of the modified GFM to multi-dimensions is rather straightforward.

## References

[1] A.M. Abd-El-Fattah, L.F. Henderson, Shock waves at a slow–fast gas interface, J. Fluid Mech. 89 (1978) 79–95.
[2] A.M. Abd-El-Fattah, L.F. Henderson, Shock waves at a fast–slow gas interface, J. Fluid Mech. 86 (1978) 15–32.

[3] R. Abgrall, How to prevent pressure oscillations in multicomponent flow calculations: a quasi-conservative approach, J. Comp. Phys. 125 (1996) 150–160.
[4] R. Abgrall, S. Karni, Computations of compressible multifluids, J. Comp. Phys. 169 (2001) 594–623.
[5] G.J. Ball, B.P. Howell, T.G. Leighton, M.J. Schofield, Shock-induced collapse of a cylindrical air cavity in water: a Free-Lagrange simulation, Shock Waves 10 (2000) 265–276.
[6] J.-P. Cocchi, R. Saurel, A Riemann problem based method for the resolution of compressible multimaterial flows, J. Comp. Phys. 137 (1997) 265–298.
[7] I.I. Glass, J.P. Sislian, Nonstationary Flow and Shock Waves, Oxford Science, 1994.
[8] J. Glimm, J.W. Grove, X.L. Li, K.-M. Shyue, Y. Zeng, Q. Zhang, Three-dimensional front tracking, SIAM J. Sci. Comput. 19 (1998) 703–727.
[9] J. Glimm, L. Xia, Y. Liu, N. Zhao, Conservative front tracking and level set algorithms, PNAS 98 (2001) 14198–14201.
[10] J. Grove, R. Menikoff, Anomalous reflection of a shock wave at a fluid interface, J. Fluid Mech. 219 (1990) 313–336.
[11] J. Falcovitz, A. Birman, A singularities tracking conservation laws scheme for compressible duct flows, J. Comp. Phys. 115 (1994) 431–439.
[12] R.P. Fedkiw, A. Marquina, B. Merriman, An isobaric fix for the overheating problem in multimaterial compressible flows, J. Comp. Phys. 148 (1999) 545–578.
[13] R.P. Fedkiw, T. Aslam, B. Merriman, S. Osher, A non-oscillatory Eulerian approach to interfaces in multimaterial flows (the Ghost Fluid Method), J. Comp. Phys. 152 (1999) 457–492.
[14] R.P. Fedkiw, T. Aslam, S. Xu, The ghost fluid method for deflagration and detonation discontinuities, J. Comp. Phys. 154 (1999) 393–427.
[15] R.P. Fedkiw, Coupling an Eulerian fluid calculation to a Lagrangian solid calculation with the ghost fluid method, J. Comp. Phys. 175 (2002) 200–224.
[16] J. Hilditch, P. Colella, A front tracking method for compressible flames in one dimension, SIAM J. Sci. Comput. 16 (1995) 755–772.
[17] P. Jenny, B. Muller, H. Thomann, Correction of conservative Euler solvers for gas mixtures, J. Comp. Phys. 132 (1997) 91–107.
[18] S. Karni, Multi-component flow calculations by a consistent primitive algorithm, J. Comp. Phys. 112 (1994) 31–43.
[19] B. Lafaurie, C. Nardone, R. Scardovelli, S. Zaleski, G. Zanetti, Modelling merging and fragmentation in multiphase flows with SURFER, J. Comp. Phys. 113 (1994) 134–147.
[20] B. Larrouturou, How to preserve the mass fractions positivity when computing compressible multi-component flow, J. Comp. Phys. 95 (1991) 31–43.
[21] T.G. Liu, B.C. Khoo, K.S. Yeo, The simulation of compressible multi-medium flow. Part I: A new methodology with applications to 1D gas–gas and gas–water cases, Comp. Fluids 30 (3) (2001) 291–314.
[22] T.G. Liu, B.C. Khoo, K.S. Yeo, The simulation of compressible multi-medium flow. Part II: Applications to 2D underwater shock refraction, Comp. Fluids 30 (3) (2001) 315–337.
[23] T.G. Liu, B.C. Khoo, K.S. Yeo, C. Wang, Shock loading in the presence of free surface and cavitation, in: The 23rd International Symposium on Shock Waves, Arlington, TX, USA, July 23–27, 2001; Int. J. Numer. Meth. Eng. (accepted).
[24] D.Q. Nguyen, R.P. Fedkiw, M. Kang, A boundary condition capturing method for incompressible flame discontinuities, J. Comp. Phys. 172 (2001) 71–78.
[25] D.Q. Nguyen, F. Gibou, R. Fedkiw, A fully conservative ghost fluid method and stiff detonation waves, in: The 12th International Detonation Symposium, San Diego, CA, 2002.
[26] M. Sussman, P. Smereka, S. Osher, A level set approach for computing solutions to incompressible two-phase flow, J. Comp. Phys. 114 (1994) 146–159.
[27] S.O. Unverdi, G. Tryggvason, A front-tracking method for viscous, incompressible, multi-fluid flows, J. Comp. Phys. 100 (1992) 25–37.
[28] Y. Zhang, K.S. Yeo, B.C. Khoo, C. Wang, 3D jet impact and toroidal bubbles, J. Comp. Phys. 166 (2001) 336–360.